BIOCHEMISTRY
including biophysical chemistry & molecular biology

Article

pubs.acs.org/biochemistry

Structural Insights into the Distinct Binding Mode of Cyclic Di-AMP with *Sa*CpaA_RCK

Ko-Hsin Chin,[†] Juin-Ming Liang,[‡] Jauo-Guey Yang,[‡] Min-Shao Shih,[‡] Zhi-Le Tu,[‡] Yu-Chuang Wang,[‡] Xing-Han Sun,[‡] Nien-Jen Hu,[‡] Zhao-Xun Liang,[§] J. Maxwell Dow,[∥] Robert P. Ryan,[⊥] and Shan-Ho Chou*[,†,‡]

[†]National Chung Hsing University Biotechnology Center, National Chung Hsing University, Taichung 40227, Taiwan, ROC

[‡]Institute of Biochemistry, National Chung Hsing University, Taichung 40227, Taiwan, ROC

[§]School of Biological Sciences, Nanyang Technological University, Singapore 637551

[∥]School of Microbiology, Biosciences Institute, University College Cork, Cork, Ireland

[⊥]Division of Molecular Microbiology, College of Life Sciences, University of Dundee, Dundee, U.K.

Supporting Information

ABSTRACT: Cyclic di-AMP (c-di-AMP) is a relatively new member of the family of bacterial cyclic dinucleotide second messengers. It has attracted significant attention in recent years because of the abundant roles it plays in a variety of Gram-positive bacteria. The structural features that allow diverse bacterial proteins to bind c-di-AMP are not fully understood. Here we report the biophysical and structural studies of c-di-AMP in complex with a bacterial cation−proton antiporter (CpaA) RCK (regulator of the conductance of K^+) protein from *Staphylococcus aureus* (*Sa*). The crystal structure of the *Sa*CpaA_RCK C-terminal domain (CTD) in complex with c-di-AMP was determined to a resolution of 1.81 Å. This structure revealed two well-liganded water molecules, each interacting with one of the adenine bases by a unique H_2O_{lp}−π interaction to stabilize the complex. Sequence blasting using the *Sa*CpaA_RCK primary sequence against the bacterial genome database returned many CpaA analogues, and alignment of these sequences revealed that the active site residues are all well-conserved, indicating a universal c-di-AMP binding mode for CpaA_RCK. A proteoliposome activity assay using the full-length *Sa*CpaA membrane protein indicated that c-di-AMP binding alters its antiporter activity by approximately 40%. A comparison of this structure to all other reported c-di-AMP−receptor complex structures revealed that c-di-AMP binds to receptors in either a "U-shape" or "V-shape" mode. The two adenine rings are stabilized in the inner interaction zone by a variety of CH−π, cation−π, backbone−π, or H_2O_{lp}−π interaction, but more commonly in the outer interaction zone by hydrophobic CH−π or π−π interaction. The structures determined to date provide an understanding of the mechanisms by which a single c-di-AMP can interact with a variety of receptor proteins, and how c-di-AMP binds receptor proteins in a special way different from that of c-di-GMP.

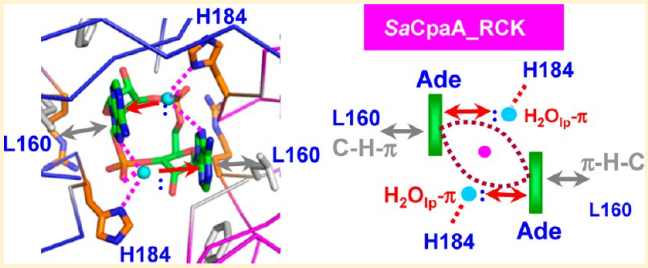

Cyclic dinucleotides are now established as important second messengers that regulate a diverse range of functions such as virulence, biofilm formation, and motility in a wide variety of bacterial species.[1−5] The best studied of these second messengers is cyclic di-GMP (c-di-GMP), which was initially described in 1987.[6] Cyclic di-AMP (c-di-AMP), which was first described in 2008 as a molecule that signals DNA integrity in *Bacillus subtilis* during sporulation,[7] is likely to be widespread in bacteria and Archaea.[8] In addition to DNA integrity monitoring, c-di-AMP is implicated in cell size and envelope stress control,[9] fatty acid synthesis regulation,[10] ion transport,[11,12] and metabolite balance.[13] An understanding of how c-di-AMP can perform such diverse but specific regulatory functions in different bacteria requires the identification of receptors for the dinucleotide and structural determination of the receptor−ligand complex. To date, a number of c-di-AMP receptors have been discovered using affinity pull-down techniques.[12−14] Nevertheless, there are relatively fewer reports about structures of c-di-AMP-bound complexes; these include the *Bs*DisA diadenylate cyclase complexed with the c-di-AMP product at the active site,[7] the TCA cycle (tricarboxylic acid cycle) enzyme pyruvate carboxylase (*Lm*PC) in complex with c-di-AMP at the allosteric site,[13] four PstA−c-di-AMP complex structures from *Staphylococcus aureus*, *B. subtilis*, or *Listeria monocytogenes*,[15−18] an HD domain phosphodiesterase PgpH in complex with c-di-AMP,[19] and the *Sa*KtrA_RCK_CTD−c-di-AMP complex structure.[20]

Received: June 10, 2015
Revised: July 14, 2015
Published: July 14, 2015

DOI: 10.1021/acs.biochem.5b00633
Biochemistry 2015, 54, 4936−4951

Recent work has implicated c-di-AMP in the regulation of ion transport in a number of bacteria.[11,12] Ion homeostasis of K^+, Na^+, and H^+ plays crucial roles in maintaining membrane potential, intracellular pH, osmoregulation, and the volume of all cells.[21,22] Ion transport proteins, including Ktr,[23] Trk,[24,25] and MthK,[21] have been investigated well to date. While the selectivity of ion transport is determined mainly by specific ion channels in the membrane-associated domain of these proteins, the ion flux rate is usually gated by a fused or separate RCK or KTN domain in the cytoplasm.[22,26] Gating of ion flux by the RCK or KTN domain is known to be controlled by two types of effectors: the Ca^{2+} ion[27,28] and adenine nucleotides such as NAD^+/NADH[29] or ATP.[30] By using an affinity pull-down assay, Corrigan and colleagues found that c-di-AMP is able to bind to KtrA (a potassium channel) and the cation−proton CpaA antiporter from *S. aureus* (*Sa*) with strong affinity in the micromolar range.[11,12] The binding region was further localized to the C-terminal domains (RCK_CTD) of these proteins.[11,12]

To gain more insight into c-di-AMP-gated ion flux, we have conducted extensive biophysical studies of the full-length *Sa*CpaA_RCK−c-di-AMP complex and determined the *Sa*CpaA_RCK−c-di-AMP and *Sa*CpaA_RCK_CTD−c-di-AMP complex structures to resolutions of 3.5 and 1.81 Å, respectively. Both structures reveal that one molecule of c-di-AMP is bound at the interface of dimeric *Sa*CpaA_RCK_CTD domains, but unexpectedly, in a region that is different from the conventional effector-binding sites of the RCK domain. Two water molecules in the interface are found to play a crucial role in binding with c-di-AMP. A proteoliposome activity assay was also conducted, using the complete *Sa*CpaA membrane protein sequence. The data indicated that c-di-AMP binding alters its antiporter activity by approximately 40%. Comparison with other reported c-di-AMP complex structures indicates commonalities but noteworthy distinct features of c-di-AMP binding to different bacterial proteins, thus providing important clues to explain why the *Sa*CpaA transporter interacts with only c-di-AMP but not c-di-GMP.

MATERIALS AND METHODS

c-di-AMP Preparation. c-di-AMP was produced from ATP by a thermophilic diadenylate cyclase enzyme. The procedures for enzymatic synthesis and product purification are similar to those described previously for c-di-GMP.[31]

Cloning, Expression, and Purification of *Sa*CpaA_RCK and Full-Length *Sa*CpaA. The coding region corresponding to *Sa*CpaA_RCK was amplified via polymerase chain reaction directly from the *S. aureus* genome. A ligation-independent cloning (LIC) approach was used to obtain the desired constructs.[32] Overexpression of the His_6 tag target protein in *Escherichia coli* strain BL21(DE3) was induced by the addition of 0.5 mM isopropyl β-D-1-thiogalactopyranoside (IPTG). The target protein was purified on a nickel column (Sigma). The His_6 tag and linker were cleaved by the tobacco etch virus (TEV) protease. Cloning and preparation of truncated *Sa*CpaA_RCK_CTD were conducted following similar procedures.

The gene encoding full-length CpaA containing the N-terminal transmembrnae region was constructed into GFP fusion vector pWaldo.[33] The plasmid was transformed into *E. coli* C43(DE3), and large scale overexpression in terrific broth (TB) was performed by 0.4 mM IPTG induction at an OD_{600} of ∼0.5 followed by a reduction of the incubation temperature to 25 °C overnight. The cell pellets were lysed with a cell disruptor from Constant System. Crude membranes were collected by ultracentrifugation at 150000*g* for 1 h. Protein extraction was conducted by adding 1% DDM in buffer containing 1× PBS (pH 7.5) and 100 mM NaCl. Solubilized *Sa*CpaA was separated by further ultracentrifugation at 150000*g* for 30 min. Initial purification was performed with a Ni-NTA column, and the GFP fusion at the C-terminus containing a His tag was cleaved by TEV protease. The purity was further polished by size exclusion chromatography using a Superdex 200 10/300 column in buffer containing 20 mM Tris (pH 7.5), 150 mM NaCl, and 0.03% DDM. Protein purity was examined by sodium dodecyl sulfate−polyacrylamide gel electrophoresis (SDS−PAGE) and concentration determined by BCA assay. Purified full-length CpaA was snap-frozen in liquid nitrogen and stored at −80 °C in a freezer before being used.

Construction of Single-Point *Sa*CpaA_RCK Variants. The *Sa*CpaA_RCK variants were constructed using the QuikChange site-directed mutagenesis kit (Stratagene),[34] using corresponding primers to introduce the L160A, R161A, I170A, and H184A substitutions. The altered proteins were expressed and purified as described above.

Biophysical Studies of the *Sa*CpaA_RCK−c-di-AMP Complex and Its Variants. The dissociation constants (K_D) of wild-type *Sa*CpaA_RCK and its variants with c-di-AMP were measured by isothermal calorimetry using an ITC200 calorimeter (MicroCal). Titrations of *Sa*CpaA_RCK proteins with c-di-AMP were conducted at 16 °C in assay buffer. Samples for ITC were dialyzed against assay buffer overnight. The c-di-AMP was diluted to 1.0 mM, and 1.5 μL of a c-di-AMP solution was injected into the cell at 3 min intervals. ITC data were fitted using a single-site binding model with the commercial package provided (Origin 7.0).

Differential scanning calorimetry (DSC) was also used to confirm the binding of *Sa*CpaA_RCK with c-di-AMP. All DSC assays to establish the midpoint melting temperature (T_m)[35] were conducted on a N-DSC III device (TA Instrument). Samples of the corresponding proteins for DSC were dialyzed extensively against assay buffer. An approximately 4.5 mg/mL (0.2 mM) protein solution with 0.4 mM ligands was transferred to the DSC sample cell. The sample was then heated at a rate of 1 °C/min from 20 to 90 °C. The molar heat capacity versus temperature was computed by using the associated program NanoAnalyze Data Analysis version 2.0 (TA Instrument).

Gel-filtration chromatography was conducted using a Sephadex 75 column. The column was calibrated by measurement of the elution volumes of the four protein markers with different molecular weights [(A) albumin, 66 kDa; (B) ovalbumin, 45 kDa; (C) myoglobin, 19 kDa; (D) cytochrome *c*, 12 kDa]. The elution volume of the target protein was used to measure the approximate molecular weight using the standard curve.

Crystallization of *Sa*CpaA_RCK and *Sa*CpaA_RCK_CTD in the Presence of c-di-AMP. For crystallization, the wild-type *Sa*CpaA_RCK protein was concentrated by using a VIVASPIN TURBO-15 instrument (Sartorius). Appropriate volumes of c-di-AMP were added to the solutions of native and *Sa*CpaA_RCK to prepare samples for cocrystallization at a ligand:protein monomer ratio of 1.5. Screening for crystallization conditions was performed using sitting-drop vapor diffusion. Initial screens were assisted using the PHENIX RE crystallization workstation (Rigaku). Crystallization of truncated *Sa*CpaA_RCK_CTD in the presence of c-di-AMP was performed in the same way.

DOI: 10.1021/acs.biochem.5b00633
Biochemistry 2015, 54, 4936−4951

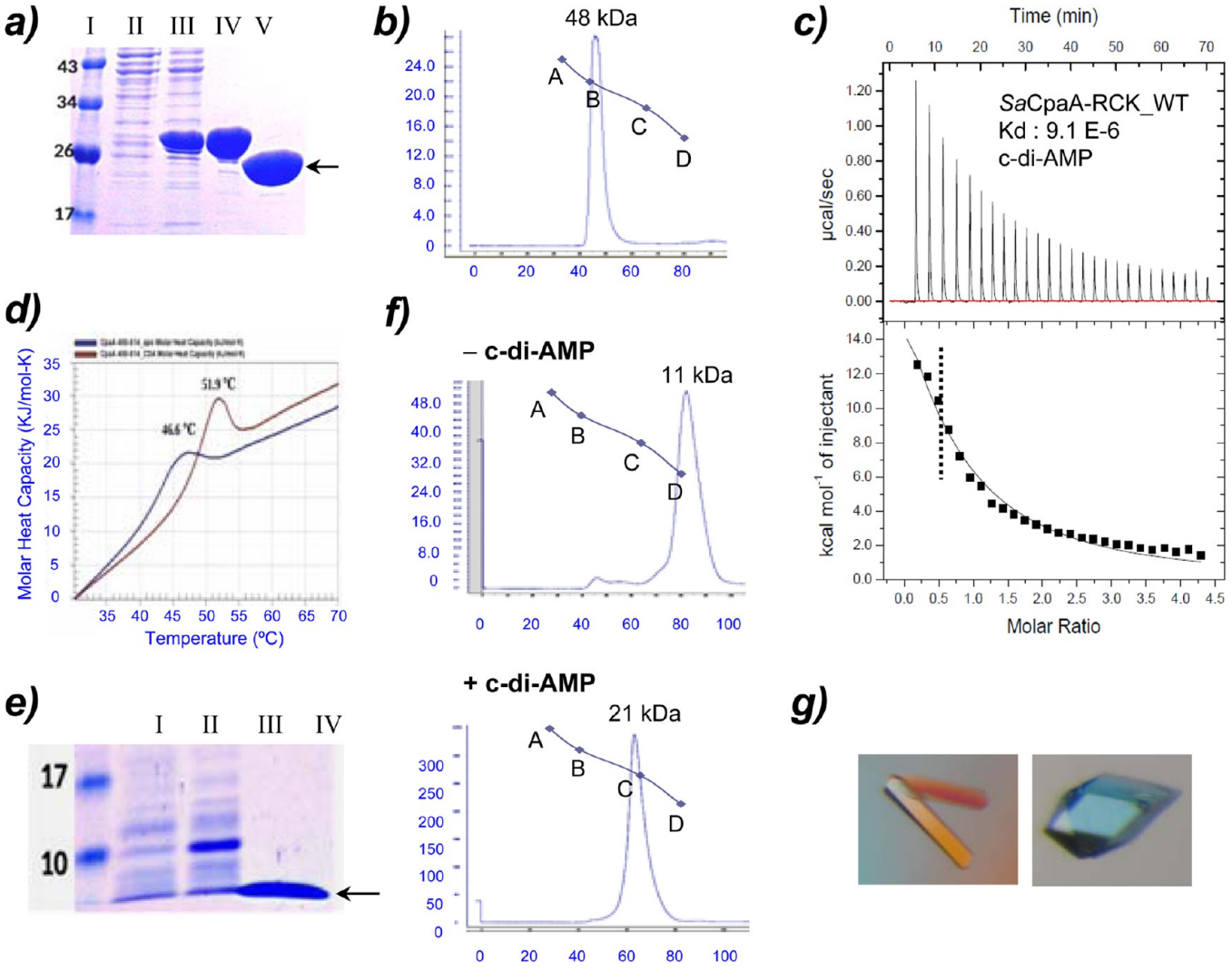

Figure 1. Purification and biophysical studies of the *Sa*CpaA RCK domain. (a) SDS−PAGE of *Sp*CpaA_RCK preparations: lane I, marker proteins; lane II, uninduced protein lysate; lane III, induced protein lysate; lane IV, purified *Sp*CpaA_RCK before tag removal; lane V, purified *Sp*CpaA_RCK after tag removal. (b) Gel-filtration chromatography shows that *Sa*CpaA RCK elutes as a dimer with a MW of 48 kDa. Capital letters indicate the elution positions of the four protein marker standards [(A) albumin, 66 kDa; (B) ovalbumin, 45 kDa; (C) myoglobin, 19 kDa; (D) cytochrome *c*, 12 kDa]. (c) An ITC study shows that it interacts with c-di-AMP with a moderate affinity (K_D ∼ 9 μM) at a ligand:protein ratio of 0.5. (d) DSC experiments show that the melting temperature of *Sp*CpaA_RCK increases by 5.3 °C after c-di-AMP binding. (e) SDS−PAGE of the preparation of the N-terminally truncated *Sp*CpaA_RCK_CTD: lane I, marker proteins; lane II, uninduced protein lysate; lane III, induced protein lysate; lane IV, purified *Sp*CpaA_RCK_CTD after tag removal. (f) Gel-filtration figures of *Sp*CpaA_RCK_CTD in the absence (top) and presence (bottom) of c-di-AMP. The truncated RCK_CTD elutes as a monomer in the absence of c-di-AMP but as a dimer when c-di-AMP is present. (g) The *Sp*CpaA_RCK_CTD−c-di-AMP complex forms either a rodlike or a rhombiclike crystal that diffracted to 1.81 Å.

Data Collection and Refinement. X-ray diffraction data for Se-Met-labeled *Sa*CpaA_RCK crystals in the presence of c-di-AMP were collected on beamline 15A1, at the National Synchrotron Radiation Research Center (NSRRC) in Taiwan. The data for the native *Sa*CpaA_RCK_CTD crystals were collected on beamline SP12B2 at the SPring-8 facility. The data were indexed and integrated using the HKL-2000 processing software. The heavy atom search, phasing, and density modification for SeMet-labeled *Sa*CpaA_RCK were conducted using the AutoSol wizard[36] from the PHENIX suite.[37] The model was manually adjusted using the XtalView/Xfit package.[38] PHENIX was then used to refine the *Sa*CpaA_RCK structure. However, because there are some regions that are disordered and could not be defined in the *Sa*CpaA_RCK_NTD, the full-length *Sa*CpaA_RCK structure could be refined to a resolution of only 3.5 Å and was considered only as a model. In contrast, the structure of the *Sa*CpaA_RCK_CTD could be determined by a molecular replacement approach of AMoRe[39] using the CTD of the lower-resolution *Sa*CpaA_RCK structure as the template, and the *Sa*CpaA_RCK_CTD−c-di-AMP complex structure was finally refined to a high resolution of 1.81 Å. Detailed data collection and refinement statistics for this higher-resolution NTD-truncated complex structure are summarized in Table 2. All structure figures were generated using PyMol.

Proteoliposome Activity Assay of the Full-Length *Sa*CpaA Antiporter. *Preparation of the Proteoliposome.* The process of reconstitution of CpaA into liposomes was modified on the basis of ref 40. In brief, 20 mg/mL L-α-phosphatidylcholine (Sigma) was dissolved in buffer 1 containing 10 mM MOPS (pH 7.3) followed by vigorous vortexing for 20 min. The lipid mix solution was aliquoted into

DOI: 10.1021/acs.biochem.5b00633
Biochemistry 2015, 54, 4936−4951

1 mL in an Eppendorf tube, and a 30 s probe sonication was performed at 40% output power followed by a 30 s incubation on ice. The lipid mix solution become clear after two sonications; 500 μL of the liposome was transferred into a new Eppendorf tube and mixed with 45 μL of sodium cholate (sigma) of a 20% stock solution and 10 μL of 65 μM purified full-length *Sa*CpaA. The contents of the Eppendorf tube were gently mixed by a rotary wheel at room temperature for 30 min. The mixture was applied to a PD-10 desalting column pre-equilibrated in buffer A. The proteoliposome was eluted in volume fractions between 4 and 6 mL to remove cholate. The eluted sample was diluted to 8 mL with buffer 1, spun by ultracentrifugation at 200000*g* for 30 min, and resuspended in 250 μL of buffer 1. Subsequently, 125 μL of proteolipsome was mixed with 1 mM pH-sensitive fluorophore pyranine (100 mM stock solution) in buffer 1 containing the desired concentration of Na_2SO_4 or K_2SO_4 inside the proteoliposome. The mixture was snap-frozen in liquid nitrogen, defrosted in a water bath, and sonicated twice for 5 s. The frost−thaw procedure was conducted again. The excessive pyranine was removed by a PD MiniTrap G-25 gel-filtration desalting column equilibrated in buffer 1 containing the desired starting concentration of Na_2SO_4 or K_2SO_4 (0.5−1 mM in the inside). The proteolipsomes were collected in void volume fractions (∼1 mL).

pH Changes Monitored by Fluorescence Measurement of Pyranine. The emission (λ_{510}) intensities of pyranine excited at 405 and 460 nm were measured using a multichannel fluorescence spectrometer (Hitachi F4500) as described (for a typical fluorescence spectrum, see Figure 3S of the Supporting Information); 200 μL of the proteoliposome was mixed with 800 μL of buffer 1 containing the same concentration of salt (no cation gradient) or a high external salt concentration (50 mM Na^+ and 100 mM K^+ on the outside), creating an inward-directed cation gradient. Then, the fluorescence emission of the mixture was immediately monitored and recorded every 10 s for 300 s. The ratios of emission (λ_{510}) intensities excited at 405 and 460 nm were calculated as F_{510}(ex. 405 nm)/F_{510}(ex. 460 nm). A decrease of the ratio indicates an increase in pH in the proteolipsomes, suggesting protons are being pumped out.[41] The effect of c-di-AMP on the CpaA antiporter activity was monitored by addition of 100 μM c-di-AMP on the outside in the presence of an inward-directed cation gradient.

RESULTS

Sequence Analysis Shows That *Sa*CpaA_RCK Lacks Some Conserved Features of RCK Domains. The RCK domain is an important element in gating the potassium ion channel. It has been well studied in recent years with several crystal structures determined, providing insights into the role that the RCK domain plays in regulating K^+ transport.[21,23,25] In *Sa*CpaA, the RCK domain is fused to a membrane-associated domain with 12 transmembrane helices.[11,12] As a first step toward understanding the regulation of the *Sa*CpaA_RCK domain, we aligned its amino acid sequence with those of the RCK domains of TrkA of *Vibrio parahemolyticus*, KtrA of *B. subtilis*, KtrA of *S. aureus*, and MthK of *Methanobacterium thermoautotrophicum* (Figure S1 of the Supporting Information). *Vp*TrkA, *Bs*KtrA, and *Sa*KtrA potassium channels are regulated by particular adenine nucleotides, whereas *Mt*MthK is regulated by Ca^{2+} ions. Surprisingly, we found that the *Sa*CpaA_RCK sequence bears little sequence identity with other RCK domain sequences (only between 14 and 17% as revealed by Dali-Lite),[42] although all five sequences contain a helix−turn−helix (HTH) domain in the central region. Importantly, *Sa*CpaA_RCK contains no GxGxxG signature motif in the N-terminal domain for binding adenine nucleotides as in the TrkA or KtrA RCK domains or a Ca^{2+}-binding motif as in the MthK RCK domain. Therefore, the *Sa*CpaA antiporter very likely adopts a noncanonical way of ion flux gating. Nevertheless, these RCK domain structures are globally similar, all adopting a "butterfly" shape as shown in Figure 2a.

Gel-Filtration Chromatography Reveals That the *Sa*CpaA_RCK Domain Exists as a Dimer. The *Sa*CpaA_RCK domain could be prepared in high yield with excellent purity after TEV cleavage (Figure 1a). The size of the product was as predicted (molecular weight of 24 kDa). During gel-filtration chromatography, *Sa*CpaA_RCK eluted as a dimer as shown by the typical profile in Figure 1b. This behavior was seen irrespective of the presence or absence of c-di-AMP or an alteration in pH conditions (data not shown). Thus, *Sa*CpaA_RCK adopts a stable dimer, unlike other RCK domains that usually associate into octamers. For examples, the MthK potassium channel gating ring[27] or the recently published TrkH−TrkA[25] and KtrA−KtrB[23] potassium transporter structures all contain a large RCK octameric structure. Because full-length *Sa*CpaA is predicted to contain 12 transmembrane helices,[12] a dimer may be sufficient to form the transmembrane channel. Nevertheless, how a *Sa*CpaA_RCK dimer would serve as a gate for regulating the antiporter activity remains to be investigated.

***Sa*CpaA_RCK Is Specific for c-di-AMP Binding.** The RCK domains in other potassium channels have been shown to regulate the potassium ion flux in response to adenine nucleotides such as ATP, NAD^+, and NADH, or Ca^{2+} ion. We were thus curious to establish whether the RCK domain in the *Sa*CpaA antiporter was able to bind these known effectors in addition to c-di-AMP. This was examined by measuring dissociation constants (K_D) using ITC. The *Sa*CpaA_RCK domain was found to bind c-di-AMP with a K_D of 9 μM at a ligand:protein ratio of 0.5, indicating that one molecule of c-di-AMP binds to a *Sa*CpaA_RCK dimer (Figure 1c). In addition, such a binding event was apparently mainly driven by entropy, as the enthalpy is very positive (Table 1). In contrast, ATP, NAD^+, and NADH or Ca^{2+} were not able to bind to the *Sa*CpaA_RCK domain with reasonable affinity (data not shown). This is consistent with the sequence analysis of the *Sa*CpaA_RCK domain (see above), which showed no sequence motif or key signature amino acid residues for binding these molecules (Figure S1 of the Supporting Information). Furthermore, c-di-GMP was also unable to bind with

Table 1. Thermodynamic Parameters of c-di-AMP Binding[a] with *Sa*CpaA_RCK and Its Variants As Measured by ITC[b]

protein	*N*	K_D	Δ*H* (kcal/mol)	Δ*S* (cal mol^{-1} K^{-1})
wild type	0.5	9.1×10^{-6}	62.8	248
R161A		5.2×10^{-4}	29.3	159
H184A		2.7×10^{-4}	23.6	36
I170A		1.1×10^{-4}	31.5	98
L160A		8.6×10^{-5}	46.9	112

[a]No or very weak binding was observed for c-di-GMP, ATP, cAMP, NADH, or Ca^{2+}. [b]All measurements were taken at pH 8.0, 20 mM Tris-HCl, and 80 mM NaCl. The obtained data were fit with a single-site binding model.

DOI: 10.1021/acs.biochem.5b00633
Biochemistry 2015, 54, 4936−4951

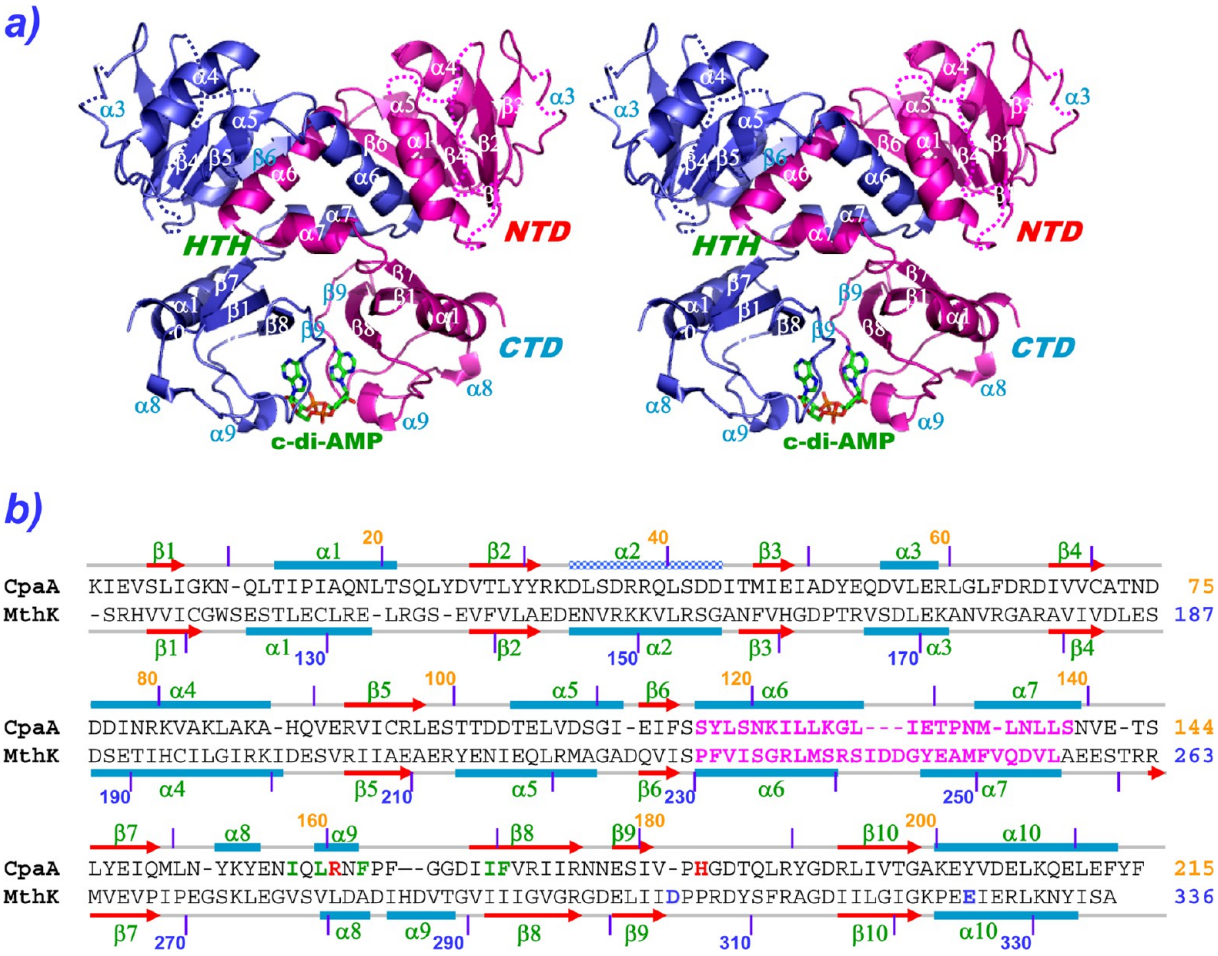

Figure 2. Structural characteristics of the *Sa*CpaA_RCK–c-di-AMP complex. (a) The structure is drawn as a ribbon, with secondary structure elements labeled. Invisible regions in the more dynamic NTD region are connected by dotted lines. The c-di-AMP (shown as balls and sticks)-bound complex structure contains a characteristic HTH domain swapping (the protomer is colored blue and magenta) in the center as a MthK–Ca^{2+} complex. (b) Structural alignment between the *Sa*CpaA_RCK–c-di-AMP and MthK–Ca^{2+} complexes. The secondary structure elements are drawn as arrows for β-strands and boxes for α-helices and are labeled sequentially. Helix α2 in the *Sa*CpaA_RCK–c-di-AMP complex is completely invisible and is shown as a dotted helix. The HTH α6–α7 domain sequences are shown as magenta text.

*Sa*CpaA_RCK [the binding was checked by ITC and DSC (data not shown)], so that the domain seems to exhibit a very high specificity for c-di-AMP.

The binding of c-di-AMP by *Sa*CpaA_RCK was further confirmed by DSC experiments. The melting temperature of the *Sa*CpaA_RCK–c-di-AMP complex (52.0 °C) was found to be higher than that of the apo form [46.6 °C (Figure 1d)]. This indicates that c-di-AMP binding enhances *Sa*CpaA_RCK_CTD stability, consistent with that determined by the ITC method (Figure 1c).

The *Sa*CpaA_RCK Crystal Structure Exhibits a HTH Domain Swapping. The full-length RCK domain from *Sa*CpaA could be cocrystallized with c-di-AMP, yet only at a lower resolution of 3.5 Å after many different trials. The crystals were found to adopt a $P3_121$ space group and contain two dimers per asymmetric unit, but the electronic density map of one of the dimers is less clear. Figure S2 of the Supporting Information shows the electronic density map of the better *Sa*CpaA_RCK dimer. In fact, its RCK_CTD domain was found to superimpose well with that of the isolated RCK_CTD structure. The full-length *Sa*CpaA_RCK molecule could be traced from the refined electron density for residues 3–213 in subunit A and residues 2–214 for subunit B, but with one major break region from residues 32–43 in subunit A and residues 32–43 in subunit B within the flexible N-terminal tail (Figure 2a). The *Sa*CpaA_RCK monomer was found to comprise three distinct domains: an N-terminal α/β domain consisting of a central five-parallel strand β-sheet packed by α-helices on both sides, a C-terminal α/β domain consisting of a central four-antiparallel strand β-sheet packed by α-helices on one side, and a linker HTH domain consisting of two α-helices (Figure 2a). These two α-helices swap the dyad twice, causing the C-terminal domain to be located on the same side of the dimer as the N-terminal domain (Figure 2a and Figure S2a of the Supporting Information). Because of the HTH domain swapping, *Sa*CpaA_RCK forms a stable dimer, with an extensive interface between the two protomers. The burial interface between them is 2681 Å^2, and that between the protein and c-di-AMP is 520 Å^2. Therefore, the formation of the *Sa*CpaA_RCK–c-di-AMP complex buries more than 3000 Å^2 of protein surface with a stabilization energy (Δ^iG) of −39.7 kcal/mol as calculated by PISA.[43] However, the NTD seems to be more flexible than the CTD, as several regions in the electron density map of RCK_NTD remain invisible (indicated by dotted lines in Figure 2a). This result indicates that apo-*Sa*CpaA_RCK is quite flexible (consistent with the result that

DOI: 10.1021/acs.biochem.5b00633
Biochemistry 2015, 54, 4936–4951

the apo form is recalcitrant to crystallization even after intensive screening) but c-di-AMP binding stabilizes its conformation mainly through its CTD. The final lower-resolution *Sa*CpaA_RCK–c-di-AMP complex structure can thus only be considered as a model because many regions at the NTD could not be sufficiently refined. Although we were still able to clearly detect the c-di-AMP density in the electron map even at a resolution of 3.5 Å (Figure S2b of the Supporting Information), it would be desirable if the complex could be determined to a better resolution. Because the lower resolution of the *Sa*CpaA_RCK–c-di-AMP complex may be possibly due to the higher flexibility of the RCK_NTD, we truncated the RCK_NTD and cocrystallized the *Sa*CpaA_RCK_CTD with c-di-AMP. This approach allowed us to obtain crystals of a c-di-AMP-bound complex that could be diffracted to 1.81 Å resolution.

The High-Resolution *Sa*CpaA_RCK_CTD–c-di-AMP Crystal Structure Reveals Detailed Interactions in the Dimeric Interface. *Sa*CpaA_RCK_CTD could be prepared and purified to homogeneity (Figure 1e). Unlike *Sa*CpaA_RCK, *Sa*CpaA_RCK_CTD no longer formed a stable dimer in the absence of c-di-AMP (Figure 1f, top) possibly because of the truncation of the NTD and central HTH domain. After incubation with c-di-AMP at a ligand:protein ratio of 1.5, *Sa*CpaA_RCK_CTD was found to form a stable dimer as revealed by gel-filtration chromatography (Figure 1f, bottom). Crystals of the *Sa*CpaA_RCK_CTD–c-di-AMP complex were successfully obtained (Figure 1g) and diffracted to a much-improved resolution of 1.81 Å (Table 2). The N-terminal truncation did not seem to change the structure of the CTD as the *Sa*CpaA_RCK_CTD–c-di-AMP complex structure can be superimposed very well with the full-length *Sa*CpaA_RCK–c-di-AMP complex structure described above, with a root-mean-square deviation of only 0.29 Å for 73 residues (not shown). Every residue in the CTD can be well traced from the N-terminus to the C-terminus, with all dihedral angles located in the most favorable region. Very low deviations of the bond angles and bond lengths are observed. The X-ray diffraction and refinement data of this shorter *Sa*CpaA_RCK_CTD–c-di-AMP complex structure are listed in Table 2.

The interface region contains polar interactions exposed to solvent and hydrophobic interactions buried inside (Figure 3a,b). The exposed polar interaction comprises two H-bonds from Thr198 γO to the side chain of Arg173, and an electrostatic interaction between the His184 side chain and the Asp168 side chain, while the buried hydrophobic interactions comprise the residues Ile170, Val172, Leu145, etc. (Figure 3b). When viewed from a different angle (Figure 3f), c-di-AMP is found to bridge well the two protomers with a well-matched electrostatic potential (Figure 3g). Specifically, the two negatively charged phosphate groups in the cyclic lactone are located in the highly positively charged region (Figure 3g). The unbiased $F_o - F_c$ electron density map of c-di-AMP in the *Sa*CpaA_RCK_CTD–c-di-AMP complex is quite visible, even when drawn at a 3σ contour level as shown in Figure 3h.

The c-di-AMP-Binding Pocket in *Sa*CpaA_RCK_CTD Reveals Two Well-Defined Water Molecules. In the *Sa*CpaA_RCK_CTD–c-di-AMP complex, c-di-AMP is well surrounded by many hydrophobic residues from above and at the side, and by polar residues from below. The hydrophobic interactions involve residues Phe165 and Leu160, Phe171 (which interacts from the side), and Ile170 (which is positioned between the adenine rings) (Figure 3b,c). Two H-bonds from the adenine ^{1}N and ^{6}NH$_2$ group also interact with the backbone atoms of Phe171 (Figure 3c). The lower electrostatic interactions involve the side chain of Arg161 with the two phosphate groups of the cyclic lactone (Figure 3c). In addition, two CH–π bond interactions from the Leu160 δ-CH$_3$ group to the adenine six-membered ring are also present (indicated by a cyan arrow in Figure 3c). However, one unexpected finding from this higher-resolution structure was the discovery that two water molecules are clearly detectable in the ligand-binding pocket and are found to significantly enhance the adenine interactions in c-di-AMP. These two specific water molecules are colored cyan in Figures 3c and 4d and indicated by white arrows in the $F_o - F_c$ electron density map shown in Figure 3h. They fill the void volume of the ligand-binding pocket when depicted as a van der Waals (space filling) model (Figure 3d,e). Each water molecule forms three H-bonds with the surrounding atoms, including the adenine ring N7 atom, the phosphate oxygen of the lactone ring, and the His184 Nδ atom (Figure 3c). In addition, the water oxygen lone pair electrons are situated above the five-membered ring of the adenine ring to form the fourth tetrahedral interaction (Figure 3c). Such

Table 2. Data Collection and Structural Refinement Statistics of the *Sa*CpaA_RCK_CTD–c-di-AMP Complex

beamline	Spring8 12B2
wavelength (Å)	1.00000
space group	$P2_12_12_1$
unit cell parameters	a = 41.49, b = 47.30, c = 70.17, $\alpha = \beta = \gamma$ = 90
resolution range (Å)	30–1.81 (1.87–1.81)[a]
total no. of observations	78975 (7835)[a]
no. of unique observations	12747 (1244)[a]
redundancy	6.2 (6.3)[a]
completeness (%)	98.9 (98.3)[a]
R_{merge}[b] (%)	3.0 (34)[a]
$I/\sigma(I)$	24.1 (2.4)[a]
R_{free} test set size (%)	5
R_{cryst},[c] R_{free}[d] (%)	20.3, 25.2
B factor	
protein residues	38.79
c-di-AMP	31.25
water	39.86
no. of residues	
protein	142
c-di-AMP	1
water	35
torsional angles[e]	
most favorable	100
root-mean-square deviation from ideal geometry	
bond lengths (Å)	0.0068
bond angles (deg)	1.14

[a]Values in parentheses are for the outermost shell, while the preceding values refer to all data. [b]$R_{merge} = \sum_{hkl}\sum_i|I_i(hkl) - \langle I(hkl)\rangle|/\sum_{hkl}\sum_i I_i(hkl)$. [c]$R_{cryst} = \sum_{hkl}||F_{obs}| - |F_{calc}||/\sum_{hkl}|F_{obs}|$, where F_{calc} and F_{obs} are the calculated and observed structure factor amplitudes, respectively. [d]R_{free} is the same as R_{cryst} but for 5.0% of the total reflections chosen at random and omitted from refinement. [e]The percentages of residues located in the most favorable and additionally allowed regions were calculated via the Molprobity program using the default parameters.[56]

DOI: 10.1021/acs.biochem.5b00633
Biochemistry 2015, 54, 4936–4951

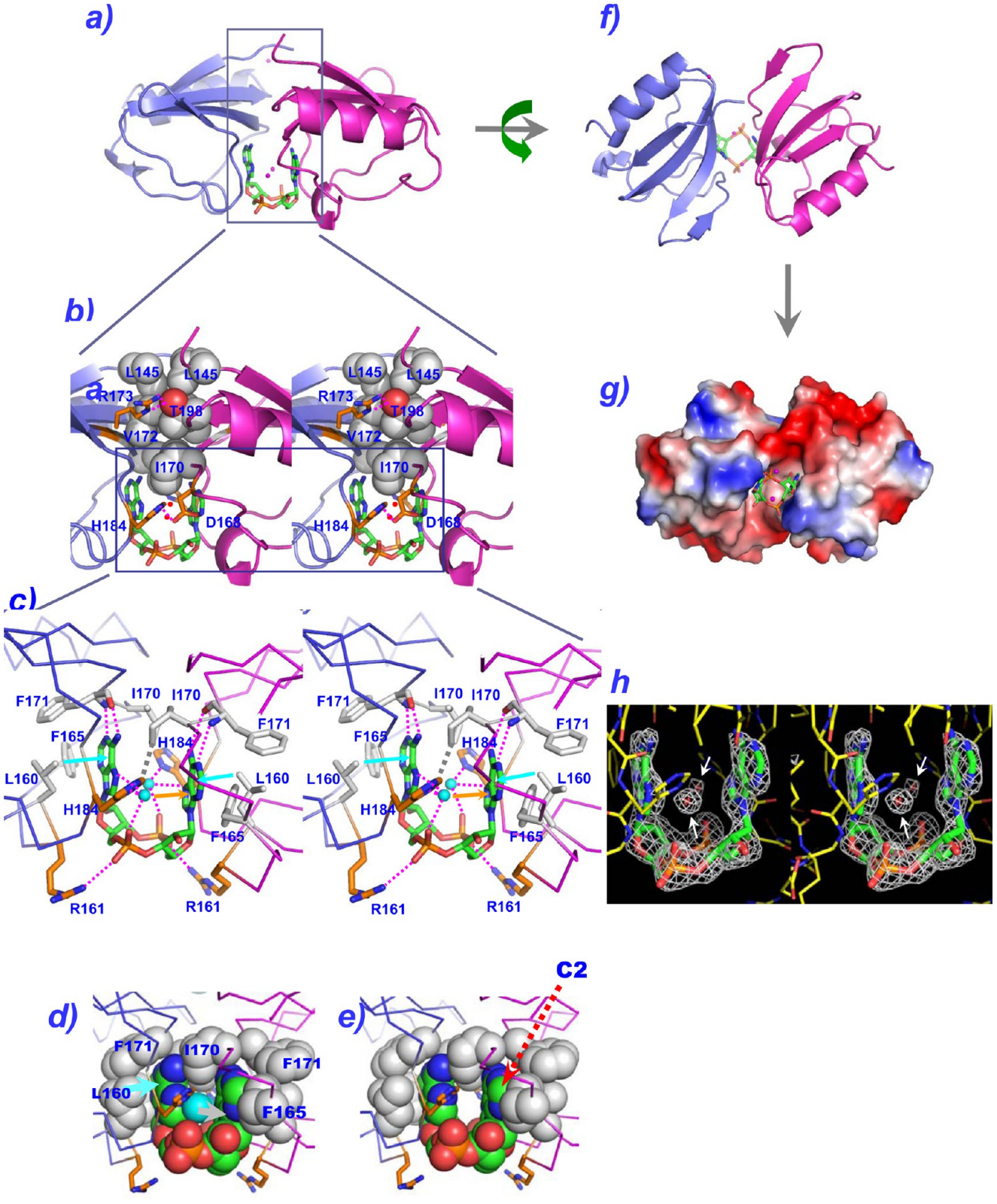

Figure 3. Structural characteristics of the prokaryotic *Sa*CpaA_RCK_CTD−c-di-AMP complex at 1.8 Å. (a) *Sa*CpaA_RCK_CTD−c-di-AMP complex dimer drawn as a ribbon, with the protomers colored blue and magenta. c-di-AMP is bound at the bottom region and drawn as balls and sticks with green carbon atoms. Two well-defined water molecules are shown as magenta dots. The boxed interface is drawn expanded in panel b in stereo. (b) The interface region comprises polar interactions exposed to solvent (polar residues are drawn as balls and sticks) and extensive hydrophobic interactions buried inside (nonpolar residues are drawn in van der Waals form in gray). The Thr198 γO atom (shown in van der Waals form in red) forms two H-bonds with the side chain of Arg173, while His184 form a polar interaction with Asp168. The ligand-binding pocket is shown expanded in panel c. (c) Detailed binding interactions in the *Sa*CpaA_RCK_CTD−c-di-AMP complex active site. Residues involved in ligand binding are drawn as balls and sticks. The carbon atoms of polar residues are colored orange, while those of hydrophobic residues are colored gray. Binding interactions are drawn as dotted magenta lines. Two water molecules are shown as cyan circles and exhibit interaction with the adenine base

DOI: 10.1021/acs.biochem.5b00633
Biochemistry 2015, 54, 4936−4951

Figure 3. continued

(shown as an orange arrow; the back one has been omitted for the sake of clarity). The outside CH−π interaction between the Leu160 methyl and adenine base is shown as a cyan arrow. (d) Similar view of the binding pocket drawn in van der Waals form to show the compactness of the bound c-di-AMP in the active site. The characteristic CH−π (marked by a cyan arrow) and O_w(lp)−π (marked by a white arrow) interactions are denoted. The two water molecules (colored cyan) fill the void volume very well. When they are removed, a large hole is present as shown in panel e. The *Sa*CpaA_RCK_CTD−c-di-AMP complex dimer is drawn in a view different from that in panel a and shown in ribbon (f) and electrostatic (g) form. The positively charged region is colored blue and the negatively charged region red. (h) Well-observed omit $F_o - F_c$ electron density map of c-di-AMP and two tightly bound waters (indicated by white arrows) of the *Sa*CpaA_RCK_CTD−c-di-AMP complex drawn at a 3σ contour level.

special water−nucleobase stacking of lone pair−π interactions is unusual, but not unprecedented, as it has been clearly detected in a high-resolution crystal structure of an RNA pseudoknot.[44]

***Sa*CpaA_RCK Variants with Alterations of Key Ligand-Binding Residues Have Reduced c-di-AMP Binding Affinities.** The determination of the *Sa*CpaA_RCK_CTD−c-di-AMP complex structure to a high resolution clearly identified amino acid residues involved in c-di-AMP binding (Figure 3c). To confirm the essential nature of these residues for c-di-AMP binding by *Sa*CpaA_RCK, several of these residues (Arg161, His184, Ile170, and Leu160) were altered individually to Ala so that the binding of c-di-AMP by these variant proteins could be examined using ITC. As shown in Table 1, these variants reveal much weaker binding of the nucleotide, with a reduction in K_D from 10- to >100-fold. These findings establish the importance of these particular residues in binding c-di-AMP.

Multiple-Sequence Alignment of *Sa*CpaA Analgoues Indicated the Active Site Residues Are Highly Conserved. Abundant evidence presented above clearly defines a special tertiary structure for the *Sa*CpaA_RCK_CTD−c-d-AMP complex, but it is important to see whether this unique c-d-AMP binding mode is also present in other bacterial CpaA antiporters and, if so, whether their active site residues are conserved. To investigate this issue, we used the *Sa*CpaA_RCK sequence to blast the microbial genome sequence database and found that there are indeed many similar CpaA sequences in other bacterial genomes. In addition, after aligning all these sequences, we found that all crucial c-di-AMP-interacting residues are highly conserved (Figure 4d). This indicates that the unique c-di-AMP binding mode of *Sa*CpaA_RCK is very likely universal among CpaA antiporters.

A Proteoliposome Activity Assay Indicated that c-di-AMP Binding Alters the *Sa*CpaA Antiporter Activity. In the absence of an inward-directed sodium gradient (Figure 5a, solid line), the ratio F_{510}(ex. 405 nm)/F_{510}(ex. 460 nm) remains nearly unchanged, suggesting no efflux or influx of protons was detected for the CpaA proteoliposomes. However, when the inward-directed sodium gradient was established, a notable decrease in the ratio was observed (Figure 5a, dashed line), indicating an increase in the pH inside the proteoliposome; i.e., protons were pumped out in the presence of a Na^+ gradient. Intriguingly, addition of 100 μM c-di-AMP in the presence of a sodium gradient leads to a further decrease in the ratio (Figure 5a, dotted line), demonstrating that c-di-AMP enhances the *Sa*CpaA proton/Na^+ antiport activity. The differences in the ratio measured at 300 s are plotted in Figure 5b. It shows that, despite not being considerably strong, adding c-di-AMP can elevate the *Sa*CpaA antiporter activity by approximately 40%. In a similar manner, *Sa*CpaA induced proton efflux in the presence of an inward-directed potassium gradient, and addition of 100 μM c-di-AMP further enhances proton/K^+ exchange (Figure 5c,d). These *in vitro* results provide evidence that *Sa*CpaA is indeed a cation−proton antiporter with no obvious specificity for Na^+ or K^+ ion, and c-di-AMP can gate the *Sa*CpaA cation−proton exchange pathway possibly via binding with its RCK_CTD.

DISCUSSION

Emerging Importance of Cyclic Dinucleotide Research. Over the past 10 years or so, cyclic nucleotides, such as c-di-GMP,[1−5] c-di-AMP,[7,8,12] and cGMP,[45−48] have emerged as important second messengers in bacterial signal transduction and regulation. A rapidly expanding body of work has described the multiple biological functions mediated by c-di-GMP and c-di-AMP in bacteria, as well as their actions as activators of the mammalian innate immune response.[49−51] It is very likely that further functions will be discovered. For cyclic di-GMP, in particular, many classes of receptor have been described and the structures of a number of c-di-GMP−receptor complex structures have been determined. For the most updated account, see the review by Chou and Galperin.[52] These structural studies have significantly enhanced our understanding of how c-di-GMP exerts its action in bacterial signal transduction and regulation. However, comparatively fewer structures of complexes between c-di-AMP and its receptors or effectors are available.[53] In this work, we have determined the *Sa*CpaA_RCK_CTD−c-di-AMP complex structure as an approach to understanding how a receptor protein can interact specifically with c-di-AMP. By comparing it with all those determined complexes reported previously, we further delineate some general structural features that may explain how c-di-AMP can specifically interact with a variety of receptor proteins.

Evidence of H_2O_{lp}−Adenine Base Interaction. An unusual feature of the *Sa*CpaRCK_CTD−c-di-AMP complex structure was the presence of water molecules in a hydrophobic environment that acts to enhance protein−c-di-AMP interactions. Although unusual, there are several lines of evidence for this rarely observed interaction. First, the electron density of the two water molecules is clearly revealed in the unbiased omit $F_o - F_c$ map (Figure 3h), so that their presence is confirmed solely from the unbiased protein electron density. Second, the two enclosed oxygen atoms exhibit lower *B* factor values of 15 and 18 compared to the value of 35 of other surrounding water molecules. In addition, the c-di-AMP adenine base atoms also show a *B* factor value (20) lower than the average value of the protein residues (30). These data indicate a potential mutual H_2O_{lp}−π interaction between the enclosed water and the adenine base. Third, we have also conducted biophysical studies of the H184A variant to examine the importance of this residue to the final complex formation. The H184A alteration significantly decreased the binding affinity of *Sa*CpaRCK with di-AMP by approximately 30-fold as measured by ITC (Table 1). The melting temperature of the complex between c-di-AMP and the *Sa*CpaRCK H184A variant was also found to decrease by approximately 5 °C as determined by the DSC method

DOI: 10.1021/acs.biochem.5b00633
Biochemistry 2015, 54, 4936−4951

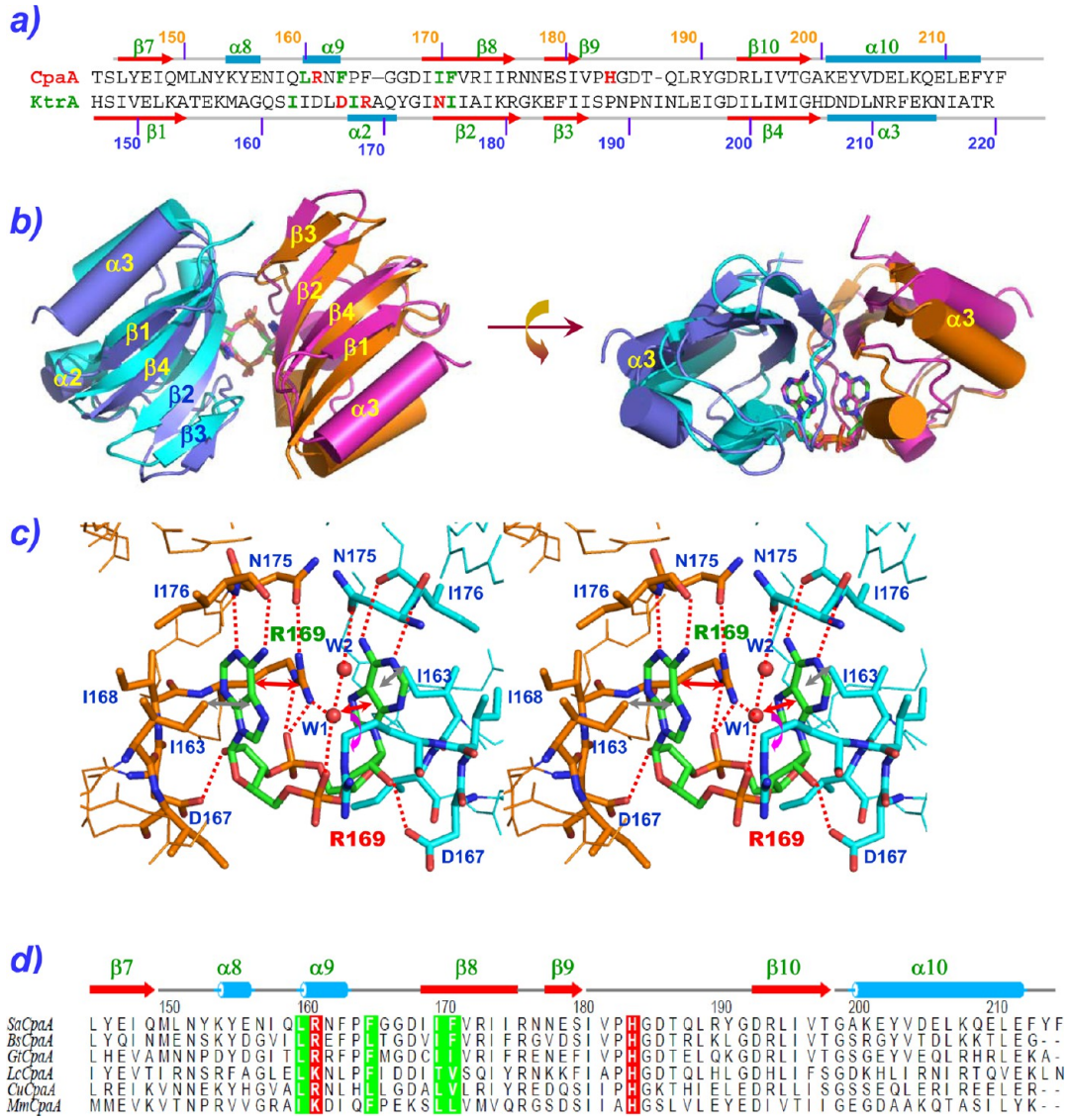

Figure 4. Structural comparison between the *Sa*CpaA_RCK_CTD−c-di-AMP and *Sa*KtrA_RCK_CTD−c-di-AMP complexes. (a) Sequence alignment between the two RCK domains. The first α-helix sequence of *Sa*KtrA_RCK_CTD was removed for comparison. The secondary structural elements of KtrA_RCK_CTD were named according to the published paper, while those of *Sa*KtrA_RCK_CTD were named similar to those in Figure 2b. The residues that participate in c-di-AMP binding are colored red for polar and green for hydrophobic. (b) Superimposition of the *Sa*CpaA_RCK_CTD−c-di-AMP and *Sa*KtrA_RCK_CTD−c-di-AMP complex structures from two different perspectives. The two protomers of the *Sa*CpaA_RCK_CTD−c-di-AMP complex are colored magenta and blue, while those of the *Sa*KtrA_RCK_CTD−c-di-AMP complex are colored orange and cyan. c-di-AMPs are drawn in stick form, with magenta and green carbon atoms. (c) Detailed binding interactions in the *Sa*KtrA_RCK_CTD−c-di-AMP complex active site. Residues involved in ligand binding are drawn as balls and sticks. The carbon atoms of participating residues are colored orange and light blue for each subunit. Binding interactions are drawn as dotted red lines. Two water molecules bound in the active site are shown as red circles. The inner-zone interactions of c-di-AMP are marked by red arrows while outer-zone interactions by gray arrows. If the torsion angle around the Cγ−Cδ bond is flipped by 180°, the guanido group of Arg169 can replace the two bound water molecules (shown by a curved magenta arrow). (d) Sequence alignment of CpaA protein homologues. The two well-conserved polar residues His184 and Arg161 or -Lys are highlighted in red and the four hydrophobic residues in green. *Bs* stands for *B. subtilis* subsp. subtilis strain RO-NN-1 (GenBank entry AEP90268.1), *Gt* for *Geobacillus thermodenitrificans* NG80-2 (GenBank entry ABO66709.1), *Lc* for *Lactobacillus casei* (NCBI reference sequence WP_047105675.1), *Cu* for *Clostridium ultunense* Esp (GenBank entry CCQ93947.1), and *Mm* for *Methanosarcina mazei* Tuc01 (NCBI reference sequence YP_007489018.1).

(data not shown). These results indicate the enclosed water needs His184 coordination to form the unique H_2O_{lp}−π interaction in the *Sa*CpaRCK−c-di-AMP complex. However, to prevent misassignment of this two-electron density to a metal ion such as Na^+ or Mg^{2+}, which exhibits a density comparable to that of a water molecule, we have further used the CheckMyMetal web server to check for the presence of other metal ions. The program can check geometry, charge, and residues surrounding different metal ions using parameters derived from a benchmark data set of quite a large number of metal-binding sites.[54] No metal ion was identified after running the program (data not shown). Taken together, these findings indicate that H_2O lone pair electrons can be accommodated in a hydrophobic environment to exert a stabilization effect in binding c-di-AMP.

DOI: 10.1021/acs.biochem.5b00633
Biochemistry 2015, 54, 4936−4951

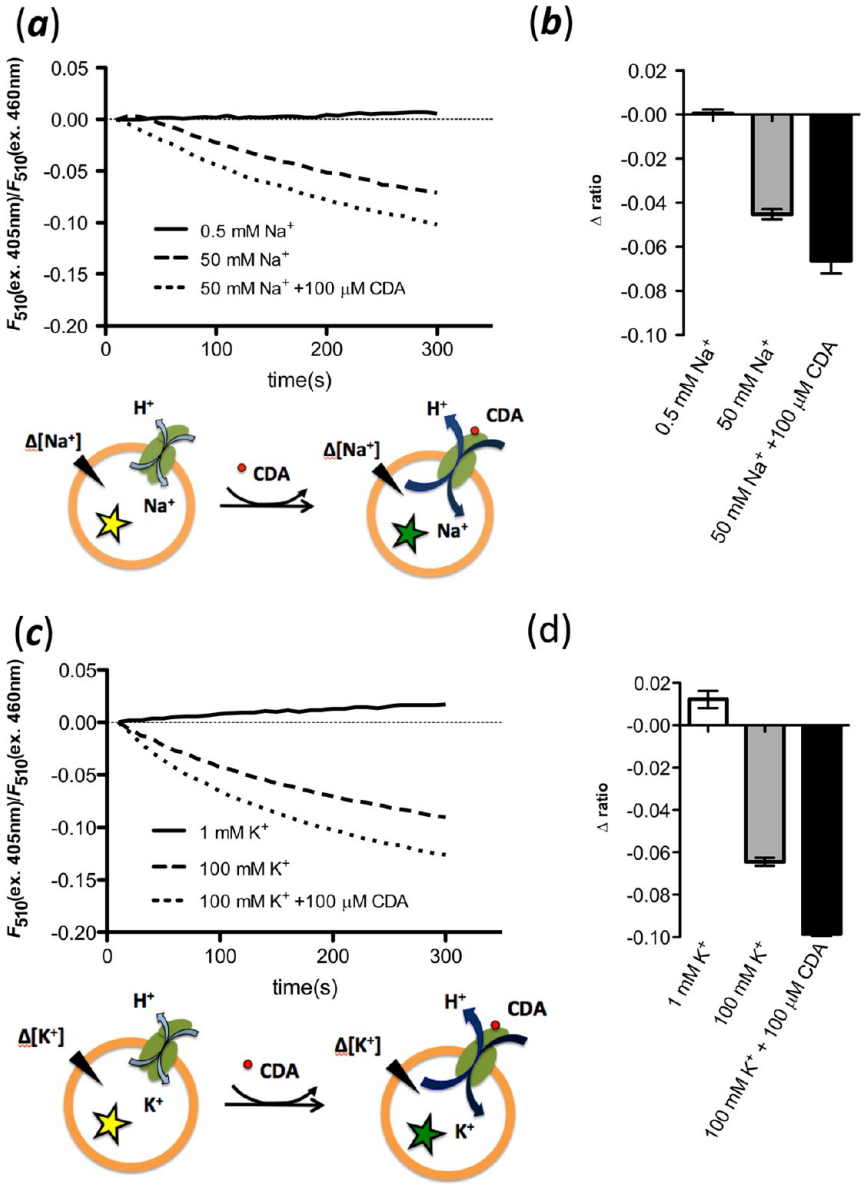

Figure 5. Cation−proton exchange of full-length CpaA using a proteoliposome containing pH-sensitive fluorophore pyranine. (a and c) The ratio of fluorescence emission (λ_{510}) intensities excited at 405 and 460 nm, respectively, is plotted vs time in the absence of an inward-directed cation gradient (—), in the presence of an inward-directed cation gradient (---), or in the presence of a cation gradient and 100 μM c-di-AMP (···). For calculation of the ratio, see Materials and Methods. (b and d) Difference in the intensity ratio (Δ ratio) measured at 300 s for the control [at 0.5 mM Na^+ or 1 mM K^+ (white bars) and 50 mM Na^+ or 100 mM K^+ (gray bars)] or 50 mM Na^+ with 100 μM c-di-AMP and 100 mM K^+ with 100 μM c-di-AMP (black bars).

Comparison of c-di-AMP Binding between *Sa*KtrA_RCK_CTD and *Sa*CpaA_RCK_CTD. The *Sa*KtrA_RCK_CTD−c-di-AMP complex structure was recently determined.[20] As this protein also contains a RCK domain that acts as a gate for K^+ transportation, it was thus interesting to compare how c-di-AMP binds to these two regulators. *Sa*KtrA and *Sa*CpaA have rather different primary sequences, with their RCK_CTD sequences sharing a similarity value of only 15% after sequence alignment (Figure 4a). They do adopt quite similar overall tertiary structures, however, both comprising a main antiparallel $\beta3\uparrow\beta2\downarrow\beta4\uparrow\beta1\downarrow$ β-sheet in close contact with a long $\alpha3$ helix (Figure 4b). In addition, both RCK_CTD domains form mainly symmetrical dimers, with a c-di-AMP molecule acting as a molecular glue. Thus, c-di-AMP binding stabilizes the RCK proteins, as revealed by the increasing melting temperature of the *Sa*CpaA_RCK domain in the presence of c-di-AMP (Figure 1d), as well as by the formation of a stable *Sa*CpaA_RCK_CTD dimer via gel-filtration chromatography upon co-incubation with c-di-AMP (Figure 1f).

However, a detailed investigation into the binding interaction reveals significant differences between the two RCK_CTD domains. As shown in Figure 4a, the polar residues participating in binding c-di-AMP are very different and located in different positions. This feature is also reflected in the rather different interaction patterns between the *Sa*KtrA_RCK_CTD− and *Sa*CpaA_RCK_CTD−c-di-AMP complexes (Figure 4c vs Figure 3c). Three noteworthy features for the *Sa*KtrA_RCK_CTD−c-di-AMP complex are apparent. First, *Sa*KtrA_RCK_CTD uses the terminal guanido group of

DOI: 10.1021/acs.biochem.5b00633
Biochemistry 2015, 54, 4936−4951

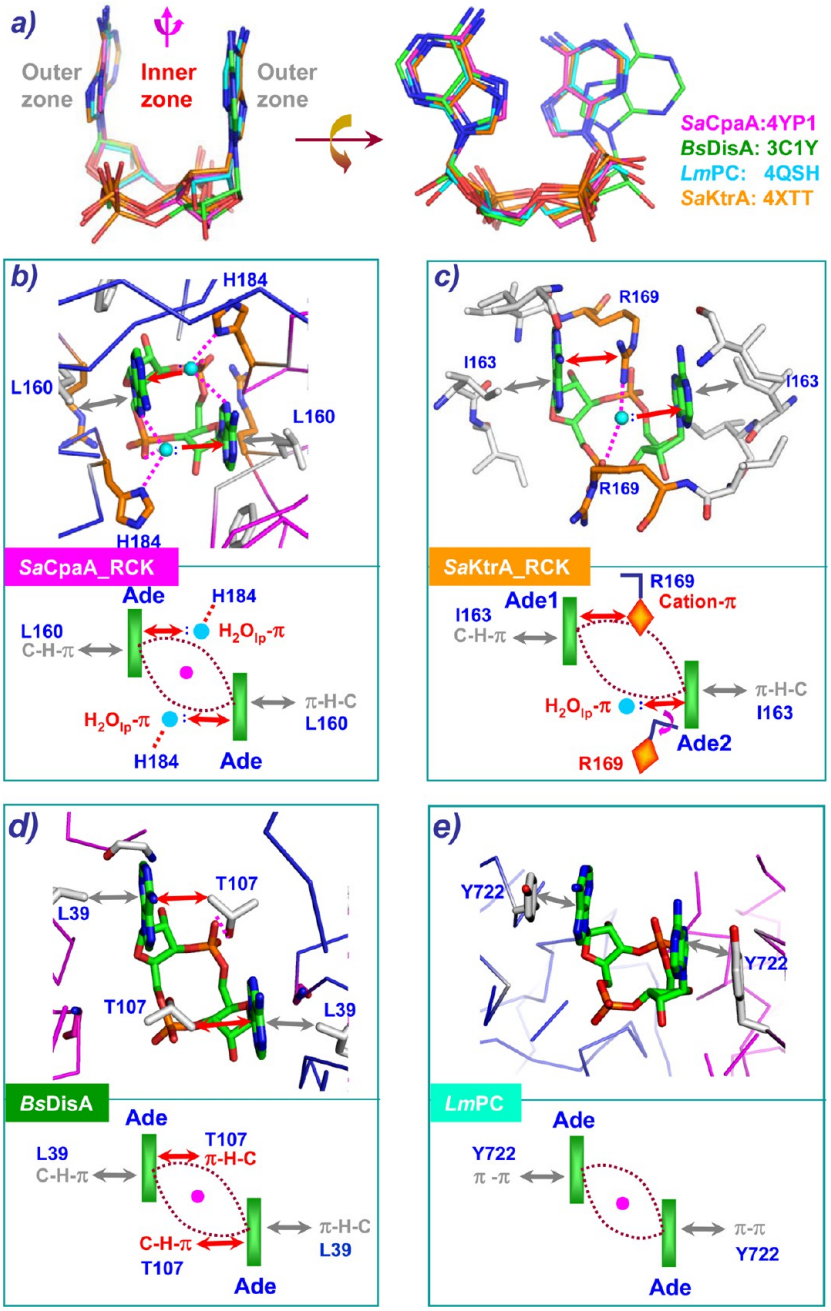

Figure 6. (a) Overlapped "U-shape" c-di-AMPs found in a variety of receptors. They exhibit similar yet distinct ways and are shown in both structural mode (top) and simplified scheme mode (bottom) for (b) *Sa*CpaA_RCK_CTD−c-di-AMP [Protein Data Bank (PDB) entry 4YP1], (c) *Sa*KtrA_RCK_CTD−c-di-AMP (PDB entry 4XTT), (d) *Bs*DisA−c-di-AMP (PDB entry 3C1Y), and (e) *Lm*PC−c-di-AMP (PDB entry 4QSH) complexes. All participating residues and c-di-AMP are drawn as sticks, and the inner interactions are shown by red arrows and the outer interactions by gray arrows. The outer-zone interactions are mainly achieved by CH−π (Figure 5b−d) or π−π interactions (Figure 5e), while the inner-zone interactions are more variable, achieved by unique H_2O_{lp}−π (Figure 5b), cation−π (Figure 5c), CH−π (Figure 5d), or no interactions (Figure 5e).

Arg169 (colored green in Figure 4c) to stack on one of the adenine bases. Second, Arg169 from another protomer (colored red in Figure 4c) is rotated by 180° to prevent its terminal guanido group from collision with the first Arg169 (this is marked by a curved magenta arrow in Figure 4c). Hence, these two arginine residues in *Sa*KtrA_RCK_CTD bind c-di-AMP in a nonsymmetrical way. Third, two water molecules, W1 and W2 (shown as red balls in Figure 4c), fill in and are located at a similar location to replace the switched-out Arg169 guanido NH1 and NH2 nitrogen atoms to participate in binding with c-di-AMP. This unique interaction pattern of c-di-AMP is very different from that used by the *Sa*CpaA_RCK_CTD−c-di-AMP complex shown in Figure 3c, in which there is no arginine residue involved in stacking or binding with the adenine base. Instead, two water molecules, each coordinated by His184 ND1, the cyclic phosphate OP1 lactone oxygen atom, and the adenine base N7 atom form the three corners of a tetrahedron, with the fourth corner of lone pair electrons interacting with the adenine base (Figure 3c). There is also no polar residue such as Asn175 that forms a H-bond with Arg169 NH1 or water molecule W2. Thus, c-di-AMP is situated in the *Sa*CpaA_RCK_CTD dimer interface in

DOI: 10.1021/acs.biochem.5b00633
Biochemistry 2015, 54, 4936−4951

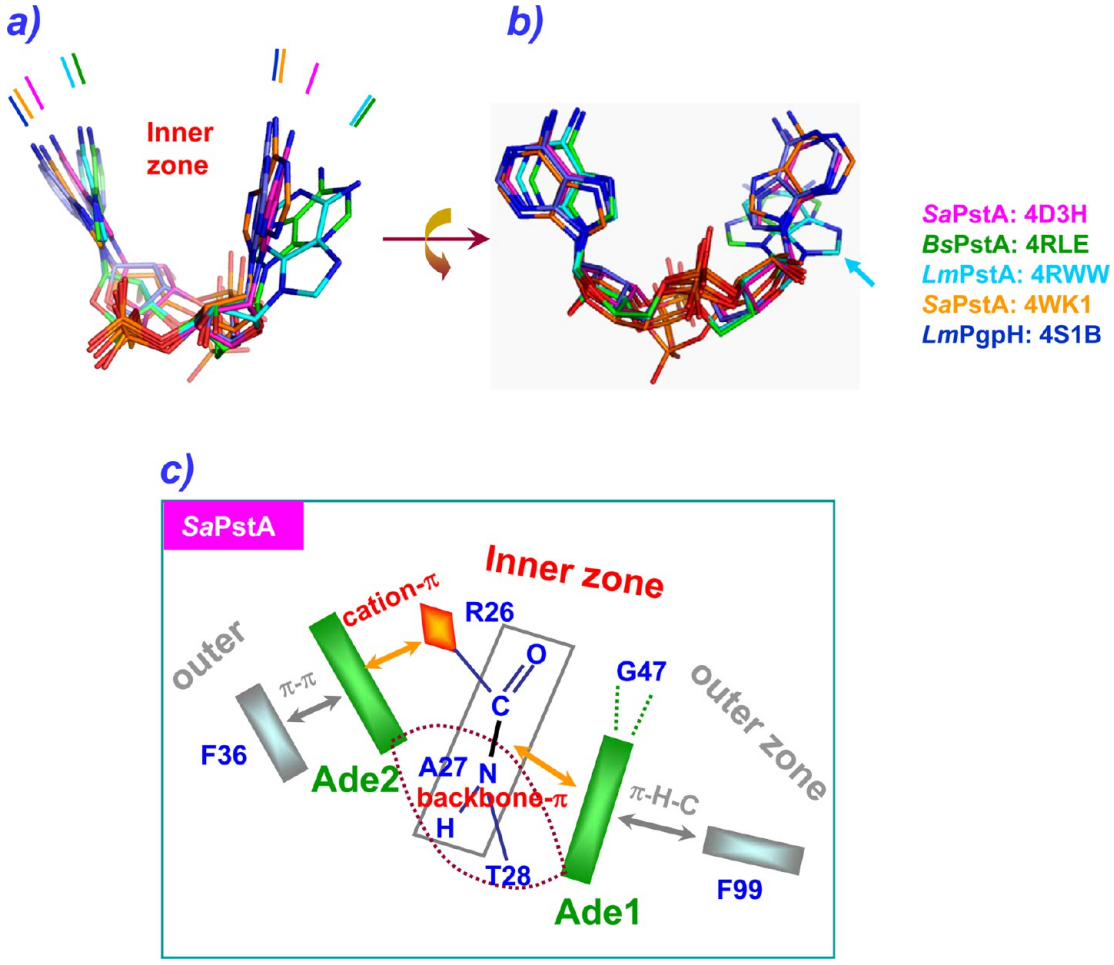

Figure 7. Overlapped "V-shape" c-di-AMP found in the *Sa*PstA (PDB entries 4D3H and 4WK1), *Bs*PstA (PDB entry 4RLE), *Lm*PstA (PDB entry 4RWW), and *Lm*HD (PDB entry 4S1B) complexes. (a) Angles between the adenine bases in the inner zone of each "V-shape" c-di-AMP are shown in different color bars. c-di-AMPs in these complexes adopt an open conformation of approximately 45°. (b) Most adenine nucleotides in the complexes adopt a *trans* conformation, while that of *Lm*PstA can adopt a *syn* conformation, indicated by a light blue arrow. (c) Scheme showing the inner- and outer-zone interactions of a typical PstA−c-di-AMP complex from *S. aureas*. A R26-A27-T28 motif runs through the top region of the "V-shape" c-di-AMP, exhibiting many unique interactions with the two adenine bases. The inner cation−π and backbone (R26-A27)−π interactions are denoted with an orange arrow, while the outer $\pi-\pi$ and CH−π interactions are denoted with gray arrows.

a symmetrical way, not asymmetrically as in the *Sa*KtrA_RCK_CTD pocket (Figure 4c). The nature of this interaction in *Sa*KtrA_RCK_CTD is not clear yet, because water W1 pairs with another W2 oxygen atom, the R169 NH1 nitrogen atom, and the cyclic phosphate OP1 oxygen atom in a planar configuration (Figure 4c), not in a tetrahedron type as found in the *Sa*CpaA_RCK_CTD structure.

Structural Comparison with Other "U-Shape" c-di-AMP-Binding Complexes. In addition to the *Sa*CpaA_RCK_CTD and *Sa*KtrA_RCK_CTD[20] domain structures, there are seven other holo c-di-AMP receptor protein structures that have been determined. These comprise four PstA complex structures from *S. aureus*, *B. subtilis*, and *L. monocytogenes*,[15,16,18,20] a c-di-AMP phosphodiesterase complex (*Lm*PgpH),[19] a pyruvate carboxylase complex (*Lm*PC) from *L. monocytogenes*,[13] and the DisA complex from *B. subtilis*.[7] When the c-di-AMP structures in all these complexes were superimposed, two major types of c-di-AMP conformation, "U shape" or "V shape", were disclosed. In the "U-shape" family (Figure 6a), the two adenine bases of c-di-AMP are oriented in an almost parallel fashion but are engaged in a variety of characteristic "inner-zone" interactions. In contrast, in the "V-shape" family (Figure 7a), the two adenine bases are inclined by approximately 45°, with the more open space in the inner interaction zone occupied by a R/G-X-T tripeptide motif (see below). It is important to note that almost all members of the "U-shape" receptor family bind c-di-AMP in a symmetrical way with a C2 axis (marked by a magenta ball in Figures 5d,e and 6b). The exception is *Sa*KtrA_RCK, which adopts a quasi-symmetrical binding mode as described in the previous section. In contrast, all "V-shape" receptor family proteins bind c-di-AMP in a nonsymmetrical way.

The symmetrical, characteristic c-di-AMP binding mode for the *Sa*CpaA_RCK receptor and its simplified scheme are shown in the top and bottom of Figure 6b, respectively. The inner interaction of bound c-di-AMP in the *Sa*CpaA_RCK_CTD-binding pocket is greatly facilitated by a pair of $H_2O_{lp}-\pi$ interactions. The outer interaction is, on the other hand, achieved mainly by Leu160 CH−π interaction surrounded by a cluster of hydrophobic amino acid residues such as Leu160, Phe165, and Phe171 (Figure 3c).

The quasi-symmetrical c-di-AMP binding mode for the *Sa*KtrA_RCK receptor is shown in Figure 6c. The reason for this nonsymmetrical behavior is unclear but may be due to the

DOI: 10.1021/acs.biochem.5b00633
Biochemistry 2015, 54, 4936−4951

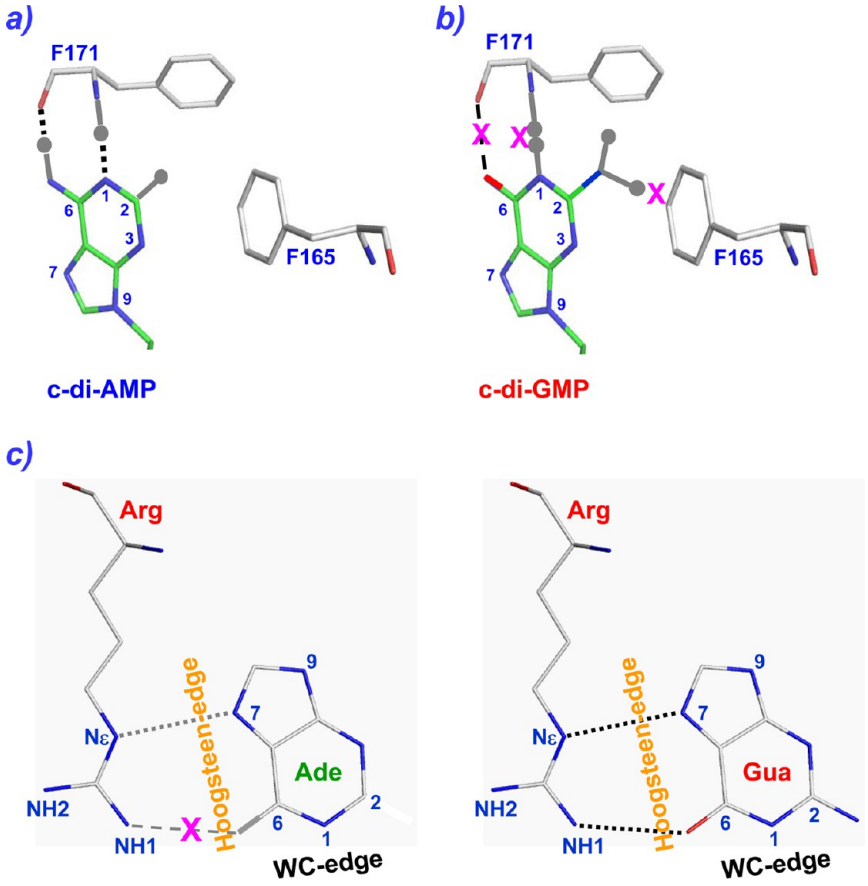

Figure 8. *Sa*CpaA_RCK_CTD binds specifically with c-di-AMP. (a) Two well-formed H-bonds between the backbone atoms of Phe171 and adenine N1 (H-bond receptor) and N6 (H-bond donor) were connected by dotted black lines, with the hydrogen atoms shown as gray balls. The adenine C2-H group can be well-accommodated in the hydrophobic cluster shown in panels c and e of Figure 3. (b) When the ligand is c-di-GMP, the guanine N1 and O6 atoms become a H-bond donor and receptor, unable to form a H-bond with the Phe171 backbone nitrogen (H-bond donor) and oxygen (H-bond receptor) atoms (marked by magenta X's), respectively. In addition, the bulky guanine $2NH_2$ group can further cause serious steric hindrance with the surrounding hydrophobic cluster as shown in panels c and e of Figure 3. (c) Hoogsteen-type binding between an adenine (left) or a guanine (right) base with the arginine terminal guanido group. Such sideways Hoogsteen arginine−adenine binding is less efficient than that between the arginine and guanine because the Ade N6 atom is also a H-bond donor.

steric hindrance and positive−positive charge repulsion between the terminal guanido groups of the two Arg169 residues. Flipping of one of the Arg169 residues and replacement with two water molecules create another type of stable inner interaction zone but at the expense of a loss of symmetry. The outer interaction zone of the *Sa*KtrA_RCK_CTD−c-di-AMP complex is created via a similar CH−π interaction pattern, comprising hydrophobic amino acid residues of Ile163, Ile168, and Ile176. Replacement of these bulky hydrophobic residues with alanines results in a substantial loss of c-di-AMP binding as measured by ITC,[20] indicating the important roles of these residues in stabilizing this complex. This is a scenario similar to that described here for the *Sa*CpaA_RCK_CTD−c-di-AMP complex, in which the binding affinity of *Sa*CpaA_RCK_CTD for c-di-AMP is significantly reduced when the crucial Leu160 is altered to an alanine (Table 1).

Figure 6d shows the c-di-AMP interaction pattern of *Bs*DisA. The inner interaction zone now comprises a simpler Thr107 CH−π interaction but is further enhanced by a Thr107 γOH−cyclic phosphate lactone OP1 interaction. In a similar way, its outer interaction zone belongs to a CH−π interaction mode, comprising Leu39, Leu94, and the Thr111 βCH_3 groups. Figure 6e shows the c-di-AMP interaction pattern of *Lm*PC, which is possibly the simplest interaction mode detected to date; no inner-zone interaction for c-di-AMP is observed, and the outer-zone interaction comprises mainly a $\pi-\pi$ interaction between the Tyr722 phenyl group and the adenine base. In addition, the two base edges of c-di-AMP seem to be exposed to solvent, making it difficult to explain why *Lm*PC is specific for c-di-AMP binding, but not for c-di-GMP binding.[13]

Structural Features of the "V-Shape" c-di-AMP-Binding Complexes. In Figure 7a, the structures of the five complexes in which c-di-AMP is bound in a "V-shape" are superimposed. In this category of protein−c-di-AMP complexes, the c-di-AMP is accommodated in a totally nonsymmetrical environment. For example, although c-di-AMP in the PstA−c-di-AMP complexes from different bacterial species is located in the trimeric interface, one adenine base (Ade1) is situated closer to the hydrophobic core of the trimer, whereas the second adenine base (Ade2) is more exposed to the solvent (Figure 7c). In the *Lm*PgpH case, only one c-di-AMP is bound in this phosphodiesterase active site, but different amino acid residues surround each adenine base. Because the four PstA−c-di-AMP complexes are more or less similar, they are discussed using the *Sa*PstA−c-di-AMP complex (PDB entry 4D3H) as the representative example. From the published structure, it is clear that an Arg26-Ala27-Thr28 motif runs through the top

DOI: 10.1021/acs.biochem.5b00633
Biochemistry 2015, 54, 4936−4951

region of the inner interaction zone between the two adenine bases, causing c-di-AMP to form a "V-shape" conformation (Figure 7c). This three-amino acid motif interacts extensively with c-di-AMP in the inner interaction zone in several ways. First, the terminal guanido group of Arg26 stacks upon the Ade2 base via the cation−π interaction. Second, the planar peptide bond between Arg26 and Ala27 stacks upon the Ade1 base to form a backbone−π interaction. Such a special stacking mode is not unprecedented and has been observed in the autoinhibition complex structure of c-di-GMP in a GGDEF domain active site.[55] Third, the Thr28 γOH group forms two bonds with the Ade1 N3 and Ade1 O2′ atoms (Figure 7c). The outer-zone interactions comprise a Phe36 stacking with an Ade2 base via the $\pi-\pi$ interaction at one end and a CH−π interaction at the other end via a Phe99 stacking upon the Ade1 base. The *Bt*PstA−c-di-AMP complex (PDB entry 4RLE) contains a similar three-amino acid motif (Arg26-Val27-Thr28) and interacts in a manner identical to that of the *Sa*PstA−c-di-AMP complex. The *Lm*PstA−c-di-AMP complex is unique in that it contains a Gly26-Ala27-Thr28 motif. It thus lacks guanido−π stacking in the inner zone. As a result, the space occupied by the long side chain atoms of Arg26 is now filled with water molecules. Nevertheless, the characteristic Gly26-Ala27 backbone interaction with the Ade2 base and the polar interaction between the Thr28 γO and Ade1 N3/Ade1 O2′ atoms are still present. Interestingly, because the more exposed Ade2 base lacks the guanido−π interaction constraint in the inner zone, it is free to switch into a *syn* conformation, which can still form a good $\pi-\pi$ interaction with Phe36. Thus, although the inner interaction zone of the *Lm*PstA−c-di-AMP complex lacks one guanido−π interaction, it can still form a stable complex when one of the adenine bases is switched into an unusual *syn* conformation. We speculate that the R/G-X-T residues may serve as a signature motif to cross-link the two adenine bases in other "V-shape" receptor−c-di-AMP complexes.

Why Does *Sa*CpaA_RCK_CTD Interact with c-di-AMP but Not c-di-GMP? To date, binding of c-di-AMP to almost all receptors has been found to involve specific interaction of the Watson−Crick (WC)-edge N1 and N6 atoms of the c-di-AMP adenine base with the backbone nitrogen and oxygen atoms of one nearby amino acid in the binding site. Figure 8a shows this interaction in *Sa*CpaA_RCK_CTD, which uses the Phe171 backbone atoms to bind to the adenine WC edge. As a typical peptide backbone comprises a H-bond donor (N−H) and a H-bond acceptor (O), it can bind very well with the complementary adenine N1 (a H-bond acceptor) and the adenine N6 (a H-bond donor) of c-di-AMP. However, substitution of c-di-AMP with c-di-GMP will completely disrupt such a favorable arrangement, as the backbone N-H atom and the guanine N1-H atom would now collide without H-bond formation, while the backbone carbonyl oxygen atom is unable to form a H-bond with the guanine O6 atom (Figure 8b). In addition, the guanine $2NH_2$ group would cause severe steric hindrance with the surrounding hydrophobic cluster amino acids (Figure 8b). The loss of favorable interactions associated with c-di-AMP binding could explain why *Sa*CpaA_RCK_CTD does not effectively bind c-di-GMP.

c-di-AMP and c-di-GMP-Binding Proteins Are Radically Different. Thus far, the only proteins that can interact with both c-di-AMP and c-di-GMP are eukaryotic receptors involved in mammalian cell innate immunity such as STING[49,50] and DDX41;[51] no bacterial protein able to bind to both of these two second messengers has been described. The structural data to date suggest some general rules about c-di-GMP binding with receptors.[52] For example, in all cases, an arginine residue is significantly involved in binding c-di-GMP and binding c-di-GMP via the guanine Hoogsteen edge (Figure 8c). Nevertheless, the c-di-GMP binding modes are quite diverse.[52] c-di-GMP can bind receptor proteins in its monomer, dimer, or even tetramer states, and the guanine bases can adopt different conformations (stacked in monomers and oligomers to fully extended monomeric forms). In contrast, the mechanism for binding of c-di-AMP differs from that of c-di-GMP, and there is no comparable diversity in c-di-AMP binding. Arginine residues are not commonly found in the c-di-AMP-binding pocket, and where they occur, they interact by stacking of the terminal guanido group onto the c-di-AMP adenine base to form a cation−π stacking, and not via the adenine Hoogsteen edge. This is possibly due to the fact that in a guanine base, its Hoogsteen edge contains O6 and N7 atoms, both of which are H-bond acceptors that can form H-bonds with the arginine terminal guanido group NH1, NH2, or NεH protons, which are H-bond donors (Figure 8c, right). In contrast, in an adenine base, the Hoogsteen edge contains a N6 amino group and a N7 atom, which are a H-bond donor and acceptor, respectively. An adenine base thus cannot form stable binding with the Arg guanido group (Figure 8c, left). Furthermore, c-di-AMP seems to interact with its receptors only in a monomeric state; as yet, no dimeric or higher-order forms have been discovered in the binding pocket. It remains to be seen whether a more diverse binding mechanism of c-di-AMP will be disclosed. From the structures determined to date, however, it appears that proteins have evolved different mechanisms for binding c-di-GMP or c-di-AMP, consistent with the fact that the two cyclic dinucleotides perform very different biological functions.

■ ASSOCIATED CONTENT

Ⓢ Supporting Information

*Sa*CpaA_RCK lacks some conserved features of regular RCK domains but contains some unique residues such as His184 that coordinates with a water molecule to form a special H_2O_{lp}−adenine interaction, and this figure clearly shows that three different ligand-binding sites are available in the various RCK domains (Figure S1); electron density map of the full-length *Sa*CpaA_RCK−c-di-AMP complex shown in stereo for one of the dimers in the asymmetric unit (Figure S2), and fluorescence emission intensities of pyranine at different excitation wavelengths (nanometers), where F_{510}(ex. 405 nm)/F_{510}(ex. 460 nm) decreases at high pH and increases at low pH (Figure S3). The Supporting Information is available free of charge on the ACS Publications website at DOI: 10.1021/acs.biochem.5b00633.

Accession Codes

The coordinates and structure factors of the *Sa*CpaA_RCK_CTD−c-di-AMP complex have been deposited as PDB entry 4YP1.

■ AUTHOR INFORMATION

Corresponding Author

*Institute of Biochemistry, National Chung-Hsing University, Taichung, 40227, Taiwan. Fax: 886-4-2285-3487. E-mail: shchou@nchu.edu.tw.

DOI: 10.1021/acs.biochem.5b00633
Biochemistry 2015, 54, 4936−4951

Funding

This work is supported in part by the Ministry of Education, Taiwan, ROC, under the ATU plan and by the Ministry of Science and Technology, Taiwan, ROC (Grant 102-2113-M-005-006-MY3) to S.-H.C. The work in the lab of Z.-X.L. is supported by a Tier II grant from the Ministry of Education of Singapore.

Notes

The authors declare no competing financial interest.

■ ACKNOWLEDGMENTS

We appreciate the service of Structural Genomics Databases provided by the GMBD Bioinformatics Core (http//www.tbi.org.tw), NRPGM, Taiwan, ROC. We also thank the Core Facilities for Protein X-ray Crystallography in the Academia Sinica, Taiwan, ROC, for help in crystal screening, the National Synchrotron Radiation Research Center (NSRRC) in Taiwan, and the SPring-8 synchrotron facility in Japan for assistance in X-ray data collection. The National Synchrotron Radiation Research Center is a user facility supported by the National Science Council, Taiwan, ROC, and the Protein Crystallography Facility is supported by the National Research Program for Genomic Medicine, Taiwan, ROC.

■ REFERENCES

(1) Hengge, R. (2009) Principles of c-di-GMP signalling in bacteria. *Nat. Rev. Microbiol. 7*, 263−273.

(2) Schirmer, T., and Jenal, U. (2009) Structural and mechanistic determinants of c-di-GMP signalling. *Nat. Rev. Microbiol. 7*, 724−725.

(3) Sondermann, H., Shikuma, N. J., and Yildiz, F. H. (2012) You've come a long way: c-di-GMP signaling. *Curr. Opin. Microbiol. 15*, 140−146.

(4) Ryan, R. P., Tolker-Nielsen, T., and Dow, J. M. (2012) When the PilZ don't work: effectors for cyclic di-GMP action in bacteria. *Trends Microbiol. 20*, 235−242.

(5) Römling, U., Galperin, M. Y., and Gomelsky, M. (2013) Cyclic di-GMP: the first 25 years of a universal bacterial second messenger. *Microbiology and Molecular Biology Reviews 77*, 1−52.

(6) Ross, P., Weinhouse, H., Aloni, Y., Michaeli, D., Weinberger-Ohana, P., Mayer, R., Braun, S., de Vroom, E., van der Marel, G. A., van Boom, J. H., and Benziman, M. (1987) Regulation of cellulose synthesis in *Acetobacter xylinum* by cyclic diguanlyate. *Nature 325*, 279−281.

(7) Witte, G., Hartung, S., Buttner, K., and Hopfner, K.-P. (2008) Structural biochemistry of a bacterial checkpoint protein reveals diadenylate cyclase activity regulated by DNA recombination intermediates. *Mol. Cell 30*, 167−178.

(8) Römling, U. (2008) Great times for small molecules: c-di-AMP, a second messenger candidate in bacteria and archaea. *Sci. Signaling 1*, pe39.

(9) Corrigan, R. M., Abbott, J. C., Burhenne, H., Kaever, V., and Grundling, A. (2011) c-di-AMP is a new second messenger in *Staphylococcus aureus* with a role in controlling cell size and envelope stress. *PLoS Pathog. 7*, e1002217.

(10) Zhang, L., Li, W., and He, Z.-G. (2013) DarR, a TetR-like transcriptional factor, is a cyclic Di-AMP-responsive repressor in *Mycobacterium smegmatis*. *J. Biol. Chem. 288*, 3085−3095.

(11) Corrigan, R. M., Campeotto, I., Jeganathan, T., Roelofs, K. G., Lee, V. T., and Gründling, A. (2013) Systematic identification of conserved bacterial c-di-AMP receptor proteins. *Proc. Natl. Acad. Sci. U. S. A. 110*, 9084−9089.

(12) Corrigan, R. M., and Gründling, A. (2013) Cyclic di−AMP: another second messenger enters the fray. *Nat. Rev. Microbiol. 11*, 513−524.

(13) Sureka, K., Choi, P. H., Precit, M., Delince, M., Pensinger, D. A., Huynh, T. N., Jurado, A. R., Goo, Y. A., Sadilek, M., Iavarone, A. T., Sauer, J.-D., Tong, L., and Woodward, J. J. (2014) The cyclic dinucleotide c-di-AMP is an allosteric regulator of metabolic enzyme function. *Cell 158*, 1389−1401.

(14) Bai, Y., Yang, J., Zarrella, T. M., Zhang, Y., Metzger, D. W., and Bai, G. (2014) Cyclic di-AMP impairs potassium uptake mediated by a cyclic di-AMP binding protein in *Streptococcus pneumoniae*. *J. Bacteriol. 196*, 614−623.

(15) Müller, M., Hopfner, K., and Witte, G. (2015) c-di-AMP recognition by Staphylococcus aureus PstA. *FEBS Lett. 589*, 45−51.

(16) Gundlach, J., Dickmanns, A., Schröder-Tittmann, K., Neumann, P., Kaesler, J., Kampf, J., Herzberg, C., Hammer, E., Schwede, F., Kaever, V., Tittmann, K., Stülke, J., and Ficner, R. (2015) Identification, characterization and structure analysis of the c-di-AMP binding PII-like signal transduction protein DarA. *J. Biol. Chem. 290*, 3069−3080.

(17) Choi, P. H., Sureka, K., Woodward, J. J., and Tong, L. (2015) Molecular basis for the recognition of cyclic-di-AMP by PstA, a P_{II}-like signal transduction protein. *MicrobiologyOpen 4*, 361−374.

(18) Campeotto, I., Zhang, Y., Mladenov, M., Freemont, P., and Gründling, A. (2015) Complex structure and biochemical characterization of the *Staphylococcus aureus* cyclic di-AMP binding protein PstA, the founding member of a new signal transduction protein family. *J. Biol. Chem. 290*, 2888−2901.

(19) Huynh, T. N., Luo, S., Pensinger, D., Sauer, J.-D., Tong, L., and Woodward, J. J. (2015) An HD-domain phosphodiesterase mediates cooperative hydrolysis of c-di-AMP to affect bacterial growth and virulence. *Proc. Natl. Acad. Sci. U. S. A. 112*, E747−E756.

(20) Kim, H., Youn, S.-J., Kim, S. O., Ko, J., Lee, J.-O., and Choi, B.-S. (2015) Structural studies of potassium transport protein KtrA regulator of conductance of K^+ (RCK) C domain in complex with cyclic diadenosine monophosphate (c-di-AMP). *J. Biol. Chem. 290*, 16393−16402.

(21) Kong, C., Zeng, W., Ye, S., Chen, L., Sauer, D. B., Lam, Y., Derebe, M. G., and Jiang, Y. (2012) Distinct gating mechanisms revealed by the structures of a multi-ligand gated K^+ channel. *eLife 1*, e00184.

(22) Lingle, C. J. (2007) Gating rings formed by RCK domains: Keys to gate opening. *J. Gen. Physiol. 129*, 101−107.

(23) Vieira-Pires, R. S., Szollosi, A., and Morais-Cabral, J. H. (2013) The structure of the KtrAB potassium transporter. *Nature 496*, 323−328.

(24) Cao, Y., Jin, X., Huang, H., Derebe, M. G., Levin, E. J., Kabaleeswaran, V., Pan, Y., Punta, M., Love, J., Weng, J., Quick, M., Ye, S., Kloss, B., Bruni, R., Martinez-Hackert, E., Hendrickson, W. A., Rost, B., Javitch, J. A., Rajashankar, K. R., Jiang, Y., and Zhou, M. (2011) Crystal structure of a potassium ion transporter, TrkH. *Nature 471*, 336−340.

(25) Cao, Y., Pan, Y., Huang, H., Jin, X., Levin, E. J., Kloss, B., and Zhou, M. (2013) Gating of the TrkH ion channel by its associated RCK protein TrkA. *Nature 496*, 317−322.

(26) Roosild, T. P., Miller, S., Booth, I. R., and Choe, S. (2002) A mechanism of regulating transmembrane potassium flux through a ligand-mediated conformational switch. *Cell 109*, 781−791.

(27) Jiang, Y., Lee, A., Chen, J., Cadene, M., Chait, B. T., and MacKinnon, R. (2002) Crystal structure and mechanism of a calcium-gated potassium channel. *Nature 417*, 515−522.

(28) Smith, F. J., Pau, V. P. T., Cingolani, G., and Rothberg, B. S. (2013) Structural basis of allosteric interactions among Ca^{2+}-binding sites in a K^+ channel RCK domain. *Nat. Commun. 4*, 2621.

(29) Kilfoil, P. J., Tipparaju, S. M., Barski, O. A., and Bhatnagar, A. (2013) Regulation of ion channels by pyridine nucleotides. *Circ. Res. 112*, 721−741.

(30) Kroning, N., Willenborg, M., Tholema, N., Hanelt, I., Schmid, R., and Bakker, E. P. (2007) ATP binding to the KTN/RCK subunit KtrA from the K^+-uptake system KtrAB of *Vibrio alginolyticus*. *J. Biol. Chem. 282*, 14018−14027.

(31) Rao, F., Pasunooti, S., Ng, Y., Zhuo, W., Lim, L., Liu, A. W., and Liang, Z.-X. (2009) Enzymatic synthesis of c-di-GMP using a thermophilic diguanylate cyclase. *Anal. Biochem. 389*, 138−142.

DOI: 10.1021/acs.biochem.5b00633
Biochemistry 2015, 54, 4936−4951

(32) Wu, Y.-Y., Chin, K.-H., Chou, C.-C., Lee, C.-C., Shr, H.-L., Lyu, P.-C., Wang, A. H.-J., and Chou, S.-H. (2005) The Cloning, purification, crystallization, and preliminary X-ray crystallographic analysis of XC847, a 3′-5′ oligoribonuclease from *Xanthomonas campestris*. *Acta Crystallogr., Sect. F: Struct. Biol. Cryst. Commun. F61*, 902−905.
(33) Drew, D., Lerch, M., Kunji, E., Slotboom, D.-J., and de Gier, J.-W. (2006) Optimization of membrane protein overexpression and purification using GFP fusions. *Nat. Methods 3*, 303−313.
(34) Vandeyar, M. A., Weiner, M. P., Hutton, C. J., and Batt, C. A. (1988) A simple and rapid method for the selection of oligodeoxynucleotide-directed mutants. *Gene 65*, 129−133.
(35) Bruylants, G., Wouters, J., and Michaux, C. (2005) Differential scanning calorimetry in life science: thermodynamics, stability, molecular recognition and application in drug design. *Curr. Med. Chem. 12*, 2011−2020.
(36) Terwilliger, T. C., Adams, P. D., Read, R. J., McCoy, A. J., Moriarty, N. W., Grosse-Kunstleve, R. W., Afonine, P. V., Zwart, P. H., and Hung, L.-W. (2009) Decision-making in structure solution using Bayesian estimates of map quality: the PHENIX AutoSol wizard. *Acta Crystallogr., Sect. D: Biol. Crystallogr. D65*, 582−601.
(37) Adams, P. D., Afonine, P. V., Bunkoczi, G. b., Chen, V. B., Davis, I. W., Echols, N., Headd, J. J., Hung, L.-W., Kapral, G. J., Grosse-Kunstleve, R. W., McCoy, A. J., Moriarty, N. W., Oeffner, R., Read, R. J., Richardson, D. C., Richardson, J. S., Terwilliger, T. C., and Zwar, P. H. (2010) PHENIX: a comprehensive Python-based system for macromolecular structure solution. *Acta Crystallogr., Sect. D: Biol. Crystallogr. D66*, 213−221.
(38) McRee, D. E. (1999) XtalView/Xfit - A versatile program for manipulating atomic coordinates and electron density. *J. Struct. Biol. 125*, 156−165.
(39) Navaza, G. (1994) AMoRe: an automated package for molecular replacement. *Acta Crystallogr., Sect. A: Found. Crystallogr. A50*, 157−163.
(40) Lee, C., Kang, H. J., von Ballmoos, C., Newstead, S., Uzdavinys, P., Dotson, D. L., Iwata, S., Beckstein, O., Cameron, A. D., and Drew, D. (2013) A two-domain elevator mechanism for sodium/ proton antiport. *Nature 501*, 573−577.
(41) Aguedo, M., Wache, Y., and Belin, J. M. (2001) Intracellular pH-dependent efflux of the fluorescent probe pyranine in the yeast *Yarrowia lipolytica*. *FEMS Microbiol. Lett. 200*, 185−189.
(42) Holm, L., and Rosenstrom, P. (2010) Dali server: conservation mapping in 3D. *Nucleic Acids Res. 38*, W545−W549.
(43) Krissinel, E., and Henrick, K. (2007) Inference of macromolecular assemblies from crystalline state. *J. Mol. Biol. 372*, 774−797.
(44) Sarkhel, S., Rich, A., and Egli, M. (2003) Water-nucleobase ″stacking″: H-π and lone pair-π Interactions in the atomic resolution crystal structure of an RNA pseudoknot. *J. Am. Chem. Soc. 125*, 8998−8999.
(45) Marden, J. N., Dong, Q., Roychowdhury, S., Berleman, J. E., and Bauer, C. E. (2011) Cyclic GMP controls *Rhodospirillum centenum* cyst development. *Mol. Microbiol. 79*, 600−615.
(46) An, S.-Q., Chin, K.-H., Febrer, M., McCarthy, Y., Yang, J.-G., Liu, C.-L., Swarbreck, D., Rogers, J., Maxwell Dow, J., Chou, S.-H., and Ryan, R. P. (2013) A cyclic GMP-dependent signalling pathway regulates bacterial phytopathogenesis. *EMBO J. 32*, 2430−2438.
(47) Gomelsky, M. (2011) cAMP, c-di-GMP, c-di-AMP and now cGMP: bacteria use them all! *Mol. Microbiol. 79*, 562−565.
(48) Gomelsky, M., and Galperin, M. Y. (2013) Bacterial second messengers, cGMP and c-di-GMP, in a quest for regulatory dominance. *EMBO J. 32*, 2421−2423.
(49) Barber, G. N. (2014) STING-dependent cytosolic DNA sensing pathways. *Trends Immunol. 35*, 88−93.
(50) Burdette, D., Monroe, K., Sotelo-Troha, K., Iwig, J., Eckert, B., Hyodo, M., Hayakawa, Y., and Vance, R. (2011) STING is a direct innate immune sensor of cyclic di-GMP. *Nature 478*, 515−518.
(51) Parvatiyar, K., Zhang, Z., Teles, R. M., Ouyang, S., Jiang, Y., Iyer, S. S., Zaver, S. A., Schenk, M., Zeng, S., Zhong, W., Liu, Z.-J., Modlin, R. L., Liu, Y.-j., and Cheng, G. (2012) The helicase DDX41 recognizes the bacterial secondary messengers cyclic di-GMP and cyclic di-AMP to activate a type I interferon immune response. *Nat. Immunol. 13*, 1155−1161.
(52) Chou, S.-H., and Galperin, M. Y. (2015) Diversity of c-di-GMP-binding proteins and mechanisms. *J. Bacteriol.*, JB.00333-15.
(53) Commichau, F. M., Dickmanns, A., Gundlach, J., Ficner, R., and Stulke, J. (2015) A jack of all trades: the multiple roles of the unique essential second messenger cyclic di-AMP. *Mol. Microbiol. 97*, 189.
(54) Zheng, H.-B., Chordia, M. D., Cooper, D. R., Chruszcz, M., Muller, P., Sheldrick, G. M., and Minor, W. (2013) Validation of metal-binding sites in macromolecular structures with the CheckMyMetal web server. *Nat. Protoc. 9*, 156−170.
(55) Yang, C.-Y., Chin, K.-H., Chuah, M. L.-C., Liang, Z.-X., Wang, A. H.-J., and Chou, S.-H. (2011) On the structure and inhibition of a GGDEF diguanylate cyclase complexed with $(c\text{-di-GMP})_2$ at active site. *Acta Crystallogr., Sect. D: Biol. Crystallogr. D67*, 997−1008.
(56) Chen, V., Arendall, W., Headd, J., Keedy, D., Immormino, R., Kapral, G., Murray, L., Richardson, J., and Richardson, D. (2010) MolProbity: all-atom structure validation for macromolecular crystallography. *Acta Crystallogr., Sect. D: Biol. Crystallogr. D66*, 12−21.

DOI: 10.1021/acs.biochem.5b00633
Biochemistry 2015, 54, 4936−4951